MATERIALS CHEMISTRY FRONTIERS

REVIEW

View Article Online
View Journal | View Issue

Cite this: *Mater. Chem. Front.*, 2020, **4**, 2205

Silver nanoclusters: synthesis, structures and photoluminescence†

Yun-Peng Xie, *[a] Yang-Lin Shen,[a] Guang-Xiong Duan,[a] Jun Han,[a] Lai-Ping Zhang[b] and Xing Lu *[a]

Metal nanoclusters (NCs) consist of tens to hundreds of metal atoms with a diameter of <2 nm, and have attracted significant attention due to their unique molecule-like properties, such as well-defined molecular structures, explicit HOMO–LUMO transitions, quantized charge and strong luminescence emission. Various robust synthetic protocols have been successfully applied to the preparation of metal NCs. Among metal NCs, Au NCs stay at the frontline of this research, and more structural characteristics, particular optical, catalytic and electronic properties, and related technical applications of Au NCs have been discovered in recent years. By taking guidelines from Au NC research, Ag NCs have recently received increasing attention. In this review article, we first survey recent advances in developing efficient synthetic methods for Ag NCs, highlighting the underlying physical and chemical properties that make the delicate control of their sizes and surfaces possible. In the following section, we discuss recent advances in the structural determination of Ag NCs, such as Ag_{25}(2,4-DMBT)$_{18}$ (2,4-DMBT: 2,4-dimethylbenzenethiolate), Ag_{29}(1,3-BDT)$_{12}$ (1,3-BDT: 1,3-benzenedithiolate), and $Ag_{44}(SR)_{30}$ (R = $PhCO_2H_2$, PhF, PhF_2 or $PhCF_3$). Structural determination will help to gain deep insight into the structure–property relationships at the molecular level. In the last part, we highlight some examples of Ag NCs to demonstrate their photoluminescence properties, which offer potential applications as photodetectors and in sensing and bio-imaging. We give a brief outlook on the future development of Ag NCs from the viewpoint of synthesis and applications.

Received 3rd March 2020,
Accepted 27th May 2020

DOI: 10.1039/d0qm00117a

rsc.li/frontiers-materials

1. Introduction

Atomically precise metal nanoclusters (NCs) are ultrasmall particles with core sizes below 2 nm, and they are in between the atomic regime and plasmonic metal nanoparticles.[1–7] Such metal NCs exhibit dramatically unique electronic and optical properties, such as molecule-like energy gaps, strong photoluminescence (PL) and high catalytic properties.[8–15] Among metal NCs, noble metal NCs have drawn tremendous attention from the scientific community because of their unique structures and correlation with versatile applications.[3–7] A number of magic size Au and Ag NCs with precise formulas such as $Au_{25}(SCH_2CH_2Ph)_{18}$,[16–18] $Au_{38}(SCH_2CH_2Ph)_{24}$,[19–21] and $Au_{102}(SPhCO_2H_2)_{44}$[22] as well as Ag_{25}(2,4-DMBT)$_{18}$,[23] Ag_{29}(1,3-BDT)$_{12}$,[24] and $Ag_{44}(SR)_{30}$ (R = $PhCO_2H_2$, PhF, PhF_2 or $PhCF_3$)[25,26] are known. Organic ligands such as thiolates, phosphines, and alkynyls are usually used to cap the surface in order to prevent aggregation and to facilitate the isolation of target Au and Ag NCs.[6,7,27] These ligands not only influence the formation processes of Au and Ag NCs but also determine their structures and thus sizes, shapes and eventual properties.

Among the noble metal NCs reported so far, Ag NCs are particularly attractive because of the unique physical properties of Ag NCs, such as their strong luminescence and ultra-small size. Such properties provide good platforms to construct luminescent probes for bio-imaging and sensing applications.[28,29] However, silver in the zero-valent state is more reactive and easier to oxidize than gold, which makes it more difficult to prepare Ag NCs and investigate their properties as compared with the rather intensively studied gold analogues. Thus, the accessibility of high-quality Ag NCs with well-defined size, structure and surface is crucial for both fundamental and applied science.

Recently, a number of efficient strategies have been developed for the synthesis of Ag NCs with tailorable physico-chemical properties, and also in quantities large enough for practical applications.[28,29] With delicate design of synthetic methods such as direct reduction, chemical etching and ligand exchange, many mature processes can be used to prepare high-quality Ag NCs

[a] *State Key Laboratory of Materials Processing and Die & Mould Technology, School of Materials Science and Engineering, Huazhong University of Science and Technology (HUST), Wuhan 430074, China. E-mail: xieyp@hust.edu.cn, lux@hust.edu.cn*

[b] *College of Chemistry and Chemistry Engineering, Xinxiang University, Xinxiang 453000, China*

† Electronic supplementary information (ESI) available. See DOI: 10.1039/d0qm00117a

with novel and even unprecedented properties. On the other hand, some techniques such as UV-vis absorption spectroscopy, PL emission spectroscopy, electrospray ionization mass spectrometry (ESI-MS), single crystal X-ray crystallography (SC-XRD), *etc.* have been used to characterize the physio-chemical properties and determine the total structures of Ag NCs, forming a central research direction in nanoscience.[28–30] The atomically precise nature of their structures enables the investigation of the structure–property relationship, which may further optimize their performance. One of the most important spectroscopic properties is the luminescence, which is particularly useful in biological applications. Tunable PL properties of Ag NCs by controlling the core size and the nature of ligands have been reported during the last five years.[31,32] It is therefore a focus of this review article to provide a detailed discussion on the synthesis, structures and photoluminescent properties of Ag NCs.

In this review article, we first survey the robust synthetic methods such as direct reduction, chemical etching and ligand exchange for high-quality Ag NCs reported during the last five years. Then we discuss recent advances in the determination of the crystal structure of Ag NCs with different sizes and well-defined molecular formulas. In the next section, we highlight some examples relating to the PL properties of Ag NCs. Some factors such as the core size, capping ligand, heterometal atom and temperature governing the PL properties of Ag NCs are addressed. Finally, a brief conclusion and an outlook on the future research challenges for Ag NC research will be provided.

2. Synthesis of Ag CNs

Compared to the synthesis of Au NCs, the synthesis of Ag NCs is more challenging due to their relative susceptibility in solution under atmospheric conditions. Thus, more delicate control is required to synthesize a well-defined composition of Ag NCs. Some successful attempts have been recently reported.[28,29] Some characterization techniques including laser desorption ionization (LDI), matrix assisted laser desorption ionization (MALDI), electrospray ionization (ESI) mass spectrometry (MS), SC-XRD and post-synthetic separation methodologies such as size exclusion chromatography (SEC) and polyacrylamide gel electrophoresis (PAGE) are also used to determine the composition and structures of Ag NCs.[33]

The synthesis of Ag NCs can be roughly classified into three categories: direct reduction of silver precursors in the presence of desired ligands, chemical etching and postsynthetic ligand-exchange.

2.1. Direct reduction

The direct reduction method has been successfully used to prepare Ag NCs in both organic and aqueous media. This synthetic process includes rapid reductive growth of intermediate Ag NCs and slow size focusing to monodisperse Ag NCs in a reducing agent.[34] $NaBH_4$ is commonly used as the reducing agent to synthesize Ag NCs with a variety of ligands such as thiolates, alkynyls, DNAs, peptides, proteins and polymers. A few Ag NCs, including thiol-protected Ag NCs (such as Ag_{25}(2,4-DMBT)$_{18}$[23] and Ag_{29}(1,3-BDT)$_{12}$[24]) and alkynyl-protected Ag NCs (such as Ag_{74}(PhC≡C)$_{44}$[35] and Ag_{51}(^{t}BuC≡C)$_{32}$[36]) have been successfully synthesized by using this method. However, the reduction kinetics with $NaBH_4$ are generally fast and this leads to the formation of polydisperse Ag NCs. Thus, several methods can be used to slow down the reduction kinetics of $NaBH_4$. For example, the solution pH,[37] the concentration of reducing agents,[38,39] and the solvent[40] can be used to adjust the reducing capability of $NaBH_4$. Another efficient way to slow down the reduction kinetics for Ag NC formation is to replace $NaBH_4$ with other mild reducing agents such as formic acid and DMF.[41,42] Some other techniques, such as light,[43] ultra-sonication,[44] and electricity,[45] can also be used to create a mild reducing environment for the formation of Ag NCs.

2.2. Chemical etching

Some Ag NCs can also be produced *via* a chemical etching process, where a relatively larger Ag nanoparticle (NP) is etched to form small Ag NCs.[46–48] Compared to the direct reduction method, there are fewer successful attempts reported involving the chemical etching process, since in general the latter is more time-consuming and often produces Ag NCs at lower yields. Such constraints can be partially addressed by optimizing the etching conditions, including the etching time, reaction temperature, and the ratio of etchant to Ag precursors.

An efficient synthetic protocol requires a mild etching environment that makes possible controlled formation of Ag NCs in the reaction solution. For example, an interfacial etching process was used to digest the as prepared Ag NPs to form two luminescent Ag NCs protected by mercaptosuccinic acid (H_2MSA).[49] During the reaction, Ag@(H_2MSA) NPs were employed as starting materials and converged to a mixture of Ag_8 and Ag_7 NCs in an aqueous–organic biphasic system, and such a mixture was separated using gel electrophoresis. Another example is the synthesis of the red luminescent Ag_{38} NC through the etching of large citrate-protected Ag@citrate NPs by adding excess mercaptosuccinic acid.[50] During the reaction, there is a disappearance of the plasmon feature at 420 nm, implying that that Ag@citrate NPs were converted to Ag NCs. The route provides nearly pure Ag_{38} NCs, and no byproducts were detected.

2.3. Ligand exchange

The ligand-exchange-induced size/structure transformation process is becoming an important approach in recent years. The peripheral organic ligands have a significant influence on the nuclearity, geometry, bonding and electronic transitions. Depending on the well characterized metal NC species, ligand-exchange may be partial or complete, with or without altering the metal core. In 2014, Bakr and coworkers presented a ligand-exchange method for the rapid and complete thiolate-for-thiolate exchange of $Ag_{44}(SR)_{30}$.[51] Later, they found that the ligand-exchange conversion of $Ag_{35}(SG)_{18}$ (SG: glutathionate) into Ag_{44}(4-FTP)$_{30}$ (4-FTP: 4-fluorothiophenol) is also rapid and direct, while the reverse process proceeds slowly through intermediate cluster sizes.[52] Meanwhile, the hollow structure

of Ag_{44}(4-FTP)$_{30}$ is converted to non-hollow Ag_{25}(2,4-DMBT)$_{18}$ *via* a disproportionation mechanism with the ligand-exchange method. The reverse reaction between Ag_{25}(2,4-DMBT)$_{18}$ and 4-FTP results in Ag_{44}(4-FTP)$_{30}$ by dimerization followed by a rearrangement reaction.[53] Recently, the Pradeep group has performed the rapid transformation of Ag_{59}(2,5-DCBT)$_{32}$ (2,5-DCBT: 2,5-dichlorobenzenethiolate) to other well-known Ag NCs, Ag_{44}(2,4-DCBT/4-FTP)$_{30}$, Ag_{25}(2,4-DMBT)$_{18}$ and Ag_{29}(1,3-BDT)$_{12}$(PPh_3)$_4$ (PPh_3: triphenylphosphine), by an exchange reaction with diverse thiol ligands.[54]

Other methods, such as performing the reaction in the solid state or in a gel, can also be used for the synthesis of Ag NCs. For instance, the Pradeep group developed a solid-state method to produce red-emitting thiolated $Ag_9(H_2MSA)_7$ nanoclusters.[55] This method can also synthesize thiolated $Ag_{32}(SG)_{19}$[56] and $Ag_{152}(PET)_{60}$ (PET: phenylethanethiol),[57] and selenolate-protected $Ag_{44}(SePh)_{30}$ NCs.[58] In addition, Chakraborty *et al.* applied the gel route to generate thiolated $Ag_{25}(SG)_{18}$ NCs with strong red emission.[59] The synthesis of Ag NCs has been summarized in some recent reviews.[28,29]

3. Structures of Ag NCs

Based on the reported metal NCs with a fully determined structure, it has been found that the stability and properties of metal NCs are influenced by a number of factors including their compositions, core structures and surface functionalities. Hence, it is crucial to control the sizes and geometric structures of the cores and the interfacial structures. Many Au NCs have been structurally determined by SC-XRD.[6,7] In contrast, the number of structurally determined Ag NCs has been limited due to their weaker stability, aerial oxidation, and lower purity. Some examples of structurally solved ligand-protected Ag NCs have been reported. More details about structural details are presented in Table S1 (ESI†). Most of the representative structures of Ag NCs could be considered as being built from basic kernel units such as Ag_4, Ag_6, Ag_7 and Ag_{13} polyhedrons. On the other hand, peripheral ligands including thiols, phosphines, alkynyls or their combination are used to protect Ag NCs. Here, we categorize the important studies of Ag NCs based on different surface ligands.

3.1. Thiol-protected Ag NCs

Thiol is the most widely used capping ligand in the shape controlled synthesis of Au and Ag NCs. In the reported thiol-protected Ag NCs with a fully determined structure, most of the representative structures could be categorized into the structure with a keplerate Ag icosahedron core and the structure with atoms arranged in a face-center-cubic (FCC) like pattern.

The icosahedron is perhaps the most widely observed structure in metal NCs. The first reported crystal structure of all thiol-protected Ag NCs was that of $Ag_{44}(SR)_{30}$ (R = $PhCO_2H_2$, PhF, PhF_2 or $PhCF_3$) in 2013.[25,26] The single crystal structure suggests the existence of a Ag_{32} kernel and six $Ag_2(SR)_5$ staples. The Ag_{32} kernel can further be divided into an icosahedral Ag_{12} core and a 20-silver-atom dodecahedral shell (Fig. 1a). By using such Ag_{44} as seeds, larger size $Ag_{50}(TBBM)_{30}(dppm)_6$ (TBBM: 4-*tert*-butylbenzyl mercaptan; dppm: bis(diphenylphosphino)-methane) was obtained by Zhu and coworkers.[60]

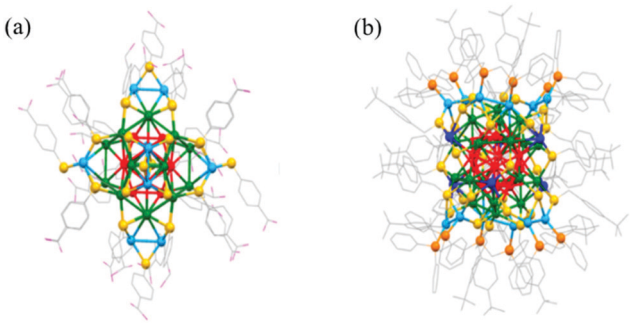

Fig. 1 Total crystal structures of the $Ag_{44}(SPhCO_2H_2)_{30}$ and the $Ag_{50}(TBBM)_{30}$-$(dppm)_6$ nanoclusters. Adapted with permission from ref. 60. Copyright 2017, American Chemical Society.

The structure of Ag_{50} comprises a Ag_{32} kernel which is retained from Ag_{44} surrounded by a dodecahedral Ag_{20} and two symmetrical $Ag_9(TBBM)_{15}P_6$ ring motifs (Fig. 1b). Subsequently, the structure of the "golden silver" Ag_{25}(2,4-DMBT)$_{18}$ NC[23] is found to be essentially identical to that of $Au_{25}(SCH_2CH_2Ph)_{18}$.[16–18] The structure of the Ag_{25}(2,4-DMBT)$_{18}$ NC has an icosahedral Ag_{13} kernel which is protected by six dimeric staples (Fig. 2a). The crystal structure of Ag_{29}(1,3-BDT)$_{12}$(Ph_3P)$_4$ protected by a dithiol and monodentate phosphine ligand has been solved by Antoine and coworkers.[24] The Ag_{29} cluster has an icosahedral core similar to that of Ag_{25}(2,4-DMBT)$_{18}$. The icosahedral core Ag_{13} is protected with a shell consisting of $Ag_{16}S_{24}P_4$ (Fig. 2b). The shell is composed of four Ag_3S_6 crowns and four $Ag_1S_3P_1$.

During the past few years, FCC core structures in metal NCs have attracted great attention due to their key roles in understanding the origin of macroscopic FCC metal materials such as gold, silver, copper, *etc.*[6,61–63] Several FCC-type kernel structures for Ag NCs have been reported thus far.

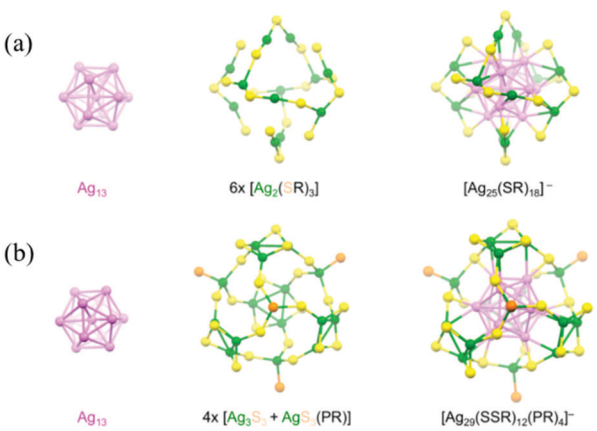

Fig. 2 Core, shell and framework of the $Ag_{25}(SPhMe_2)_{18}$ and the $Ag_{29}(BDT)_{12}(TPP)_4$ nanoclusters. Adapted with permission from ref. 6. Copyright 2016, American Chemical Society.

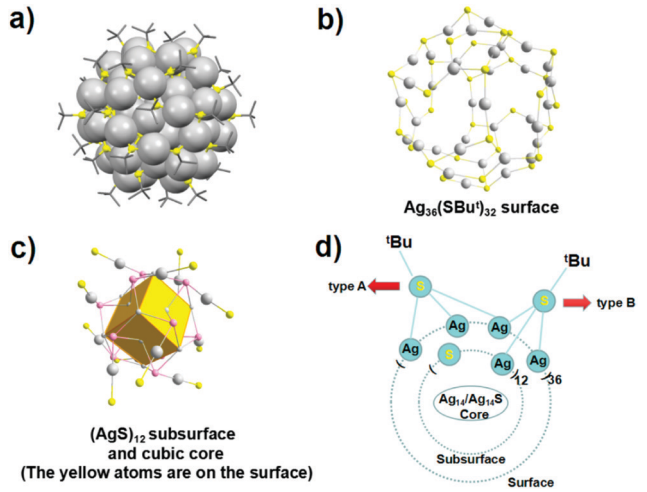

Fig. 3 X-ray structure of $[Ag_{62}S_{13}(S^tBu)_{32}]^{2+}$. (a) The similar frameworks contained in the Ag-QD, Ag-inter, and Ag-NC. (b) $Ag_{36}(S^tBu)_{32}$ shell. (c) Bonding mode of core silver atoms (gray) and sulfur atoms (pink) linked with the shell sulfur atoms (yellow). (d) Two types of ligands. Adapted with permission from ref. 66. Copyright 2016, American Chemical Society.

The FCC unit cell comprises 8 vertices and 6 face centers and, hence, a total of 14 atoms in the unit. For example, the crystal structure of an all thiol-protected $[Ag_{62}S_{12}(S^tBu)_{32}]^{2+}$ nanocluster (Ag-NC) shows a complete FCC Ag_{14} core structure with a $Ag_{48}(S^tBu)_{32}$ shell configuration interconnected by 12 sulfide ions, which is similar to the $[Ag_{62}S_{13}(S^tBu)_{32}]^{4+}$ (Ag-QD) structure.[64,65] In the center of the Ag_{14} kernel, there is an octahedral Ag_6 kernel, which is enclosed by eight equilateral-triangle-shaped planes. Of note, the Ag-QD could be electrochemically reduced into the Ag-NC, *via* an intermediate compound $[Ag_{62}S_{13}(S^tBu)_{32}]^{2+}$ (Ag-inter) (Fig. 3),[66] wherein the Ag_{62} nanocluster template remained unchanged. It can be seen that the Ag-QD, Ag-inter and Ag-NC have a similar $Ag_{36}(S^tBu)_{32}$ surface and $(AgS)_{12}$ subsurface connecting the $Ag_{36}(S^tBu)_{32}$ surface with the Ag_{14} (or $Ag_{14}S$) cubic core.

Recently, Wu *et al.* reported a new all thiol-protected $Ag_{46}S_7(2,4\text{-DMBT})_{24}$ nanocluster with FCC structure.[67] The structure of the Ag_{46} NC can be viewed as a 38-Ag atom kernel with a sulfur atom in the center, capped by surface motifs including two $Ag(2,4\text{-DMBT})_3$, six $Ag(2,4\text{-DMBT})_2$, six 2,4-DMBT, and six sulfido units. The Ag_{38} kernel can further be divided into an octahedral Ag_6 core and a 32-silver-atom tetradecahedron shell (Fig. 4). This tetradecahedron is made up of eight hexagons and six tetragons.

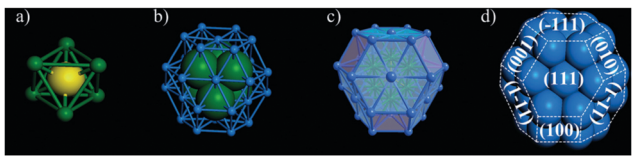

Fig. 4 (a) The central Ag_6 octahedron with a central sulfur; (b and c) the $Ag_6S@Ag_{32}$ kernel; and (d) the crystal facets of the FCC Ag_{38} kernel. S yellow, Ag other colors. Adapted with permission from ref. 67. Copyright 2018, John Wiley & Sons, Inc.

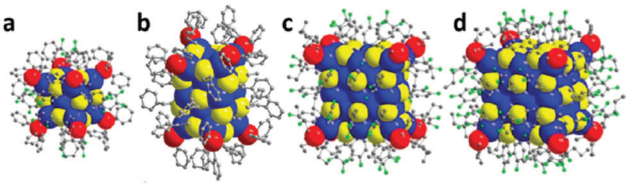

Fig. 5 X-ray structures of Ag cubes: $Ag_{14}(SC_6H_3F_2)_{12}(PPh_3)_8$, $Ag_{23}(PPh_3)_8(SC_2H_4Ph)_{18}$, $Ag_{38}(SPhF_2)_{26}(P^nBu_3)_8$, and $Ag_{63}(SPhF_2)_{36}(P^nBu_3)_8$. Adapted with permission from ref. 62. Copyright 2019, Royal Society of Chemistry.

Phosphine was usually used as an auxiliary ligand with thiol or alkyl to produce some novel metal NCs. Introducing phosphine not only enhances the yield and stability of Ag NCs but it also assists with the growth of high-quality single crystals. Thiol and phosphine ligands have excellent compatibility in protecting Ag NCs. Zheng *et al.* reported the single crystal structure of a mixed ligand protected Ag_{14} cluster in 2012.[68] As the smallest FCC-type Ag NC reported to date, the $Ag_{14}(SC_6H_3F_2)_{12}(PPh_3)_8$ cluster contains an octahedral Ag_6^{4+} core, which is encapsulated by eight cubically arranged $Ag(SC_6H_3F_2)_2PPh_3$ tetrahedrons that share one corner between them (Fig. 5a). Another important characteristic of this cluster is that all the thiolate ligands bind to three Ag atoms and no staple motifs are found. Later, a helical FCC structure was observed in the $Ag_{23}(PPh_3)_8(SC_2H_4Ph)_{18}$ nanocluster (Fig. 5b).[69] Ag_{23} has a bioctahedral Ag_{11} core, which is viewed as two Ag_6 building blocks fused together by vertex sharing. Due to a slight distortion in the vertex-sharing Ag_{11} core, Ag_{23} has a chiral structure.

When fusing four of such simple Ag_{14} FCC cubes together *via* face sharing, a square like $Ag_{38}(SPhF_2)_{26}(P^nBu_3)_8$ metal framework was obtained (Fig. 5c).[70] Further aggregation of another four Ag_{14} FCC cubes or one more square-like $Ag_{38}(SPhF_2)_{26}(P^nBu_3)_8$ gives rise to the cubic-structured $Ag_{63}(SPhF_2)_{36}(P^nBu_3)_8$ (Fig. 5d).[71]

The Zang group prepared a FCC Ag_{14} NC protected by face-capping 1,2-dithiolate-*o*-carborane ligands. Site-specific surface modification of the Ag_{14} NC with pyridyl-type ligands affords highly thermostable NCs.[72] Moreover, by using a progressively optimized ligand-bridging approach, various 1D-to-3D silver cluster-assembled materials are predesigned and obtained (Fig. 6). This strategy not only greatly improves the stability but also modulates the emission properties of the target materials.

Another series with FCC kernels pertains to the box-like $Ag_{46}(2,5\text{-DMBT})_{24}(PPh_3)_8$ and $Ag_{67}(2,4\text{-DMBT})_{32}(PPh_3)_8$ NCs.[73–75] The crystal structure of $Ag_{67}(2,4\text{-DMBT})_{32}(PPh_3)_8$ was reported by Alhilaly *et al.*[75] The Ag_{67} structure consists of a Ag_{23} kernel protected by a layer of $Ag_{44}S_{32}P_8$ arranged in the shape of a box (Fig. 7). Unlike the common Ag_{13} icosahedron geometry, the Ag_{23} kernel was formed through a cuboctahedron sharing opposite square faces with two Ag_8 crowns and then capped by two silver atoms at the open crown positions. This crowning of the Ag_{13} cuboctahedron leads to the box-shape growth of the Ag_{67} cluster. The entire cluster is stabilized by 8 AgS_3P motifs and 8 bridging thiolates. Of note, after removing a block of the $Ag_{21}(SR)_8$ unit from $Ag_{67}(SR)_{32}(PPh_3)_8$, a box-like structure of $Ag_{46}(SR)_{24}(PPh_3)_8$ was predicted. Experimentally, the $Ag_{46}(2,5\text{-DMBT})_{24}(PPh_3)_8$ NC has

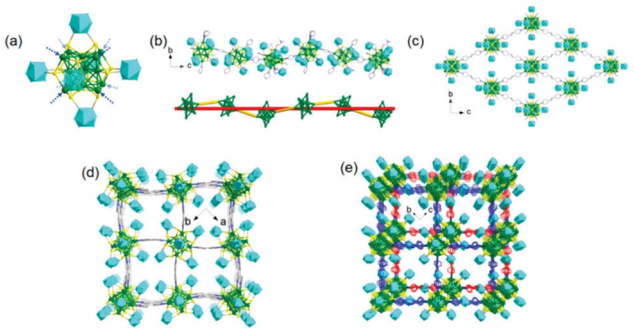

Fig. 6 Structural represention of the (a) 1,2-dithiolate-*o*-carborane-capped Ag_{14} NC; (b) 1D helix; (c) 2D grid network; (d) 3D porous framework and (e) 2-fold interpenetrated porous 3D frameworks. Adapted with permission from ref. 72. Copyright 2018, American Chemical Society.

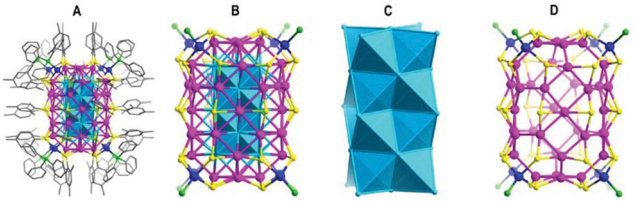

Fig. 7 (A) Total structure of $Ag_{67}(SPhMe_2)_{32}(PPh_3)_8$. (B) The structure of $Ag_{67}S_{32}P_8$ obtained by disconnecting carbon atoms in A. (C) Ag_{23} metal core. (D) The structure of the NC without the Ag_{23} metal core, *i.e.*, $Ag_{44}(SPhMe_2)_{32}(PPh_3)_8$. Adapted with permission from ref. 75. Copyright 2017, American Chemical Society.

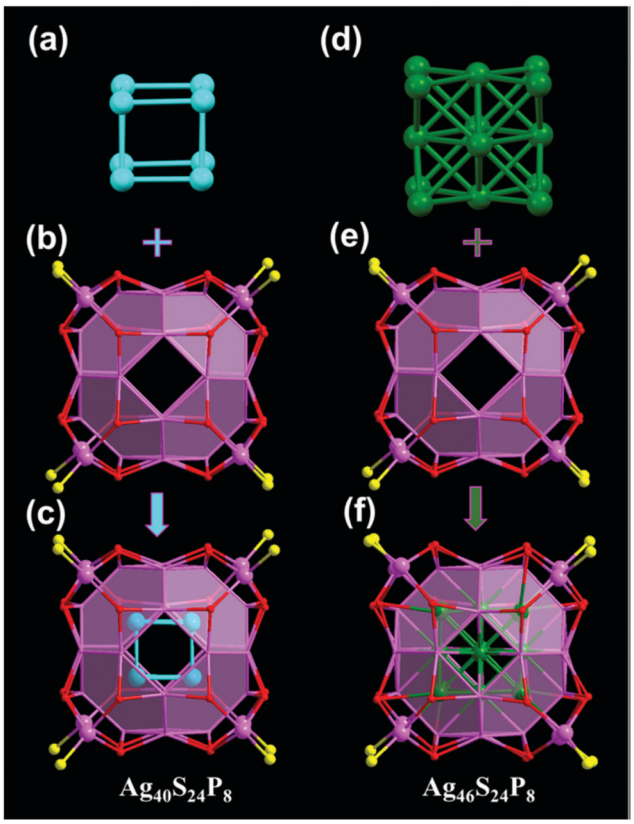

Fig. 8 Core, shell and framework of $Ag_{40}(2,4\text{-DMBT})_{24}(PPh_3)_8$ and $Ag_{46}(2,5\text{-DMBT})_{24}(PPh_3)_8$. Adapted with permission from ref. 73. Copyright 2018, American Chemical Society.

recently been synthesized and crystallized (Fig. 8).[73,74] Ag_{46} has a Ag_{14} core with a FCC structure which is protected by a $Ag_{32}S_{24}P_8$ shell.

The $Ag_{40}(2,4\text{-DMBT})_{24}(PPh_3)_8$ and $Ag_{46}(2,5\text{-DMBT})_{24}(PPh_3)_8$ NCs share the same shell of $Ag_{32}S_{24}P_8$, while the metal cores are arranged into different types (Fig. 8).[73,74] In contrast to the Ag_{46} nanocluster, Ag_{40} presents a newly found loose Ag_8 core with a simple-cubic structure. Interestingly, a cavity exists between the Ag_8 core and the inner layer of the protecting shell, but no such cavity exists in Ag_{46}. In Zhu's work, they successfully transformed Ag_{40} to Ag_{46} *via* a ligand exchange strategy.[73] Notably, the intermediate Ag nanocluster, $[Ag_{43}(2,5\text{-DMBT})_{25}(PPh_3)_4]$, was also obtained.[73] The framework of Ag_{43} has a two-shelled $Ag_{12}@A_{g20}$ core, which is protected by four kinds of units, including Ag_2S_5P, Ag_4S_8P, Ag_2S_4P and Ag_3S_6P, and two S bridge bonds were found on the surface of this nanocluster.

Recently, Zheng and coworkers reported a detailed structural and spectroscopic characterization of $Ag_{40}(DMBT)_{24}(PPh_3)_8H_{12}$ ($Ag_{40}H_{12}$).[76] In contrast to the Ag_{40} NC, the metal framework of $Ag_{40}H_{12}$ also consists of identical $Ag_8@Ag_{32}S_{24}P_8$. Based on a detailed analysis of the structural features and ^1H and ^2H NMR spectra, the positions of the 12 hydrides were determined to be residing on the 12 edges of the cubic core.

Among thiolate protected metal NCs, chiral thiolate protected metal NCs with different electronic configurations are of great importance in nanoscience and nanotechnology owing to their chiro-optical properties and applications in asymmetric drugs, sensors, and catalysts. For example, a range of structures and properties of chiral thiolate protected Au NCs including $Au_{20}(SPh^tBu)_{16}$,[77] $Au_{28}(SPh^tBu)_{20}$,[78] $Au_{38}(SCH_2CH_2Ph)_{24}$,[21] $Au_{102}(p\text{-MBA})_{44}$,[22] and $Au_{133}(SPh^tBu)_{52}$[79] have recently been studied.

We herein highlight recent findings on chiral thiolate-protected Ag NC clusters. A few chiral thiolate protected Ag NCs such as $Ag_{16}(dppe)_4(SPhF_2)_{14}$ (dppe: 1,2-bis(diphenylphosphino)ethane),[80] $Ag_{32}(dppe)_5(SPhCF_3)_{24}$,[80] $Ag_{32}(dppm)_5(SAdm)_{13}Cl_8$,[82] $Ag_{45}(dppm)_4(S^tBu)_{16}Br_{12}$,[82] and $Ag_{33}(SCH_2CH_2Ph)_{24}(PPh_3)_4$[83] have been characterized by SCXRD, in which all the surface organic ligands are achiral.

In 2003, Zheng *et al.* reported two chiral AgNCs, $Ag_{16}(dppe)_4(SPhF_2)_{14}$ and $Ag_{32}(dppe)_5(SPhCF_3)_{24}$,[80] which are protected by achiral diphosphine and thiolate ligands. The clusters have core–shell structures with a multinuclear Ag unit encapsulated in a shell containing a Ag(I)–thiolate–diphosphine complex. In $Ag_{16}(dppe)_4(SPhCF_2)_{14}$, a Ag_8 core is encapsulated in a shell of $Ag_8(dppe)_4(SPhCF_2)_{14}$, while the structure of $Ag_{32}(dppe)_5(SPhCF_3)_{24}$ shows that it possesses a Ag_{22} core protected by one $Ag_6(dppe)_3(SPhCF_3)_{12}$, two $Ag_2(dppe)(SPhCF_3)_4$ and four $(SPhCF_3)$ units. As shown in Fig. 9, both Ag_{16} and Ag_{32} conform to C_2 symmetry, and their chirality is caused by the asymmetric arrangements of the tetrahedral $[AgS_3P]$ coordination units on the surface.

As a further development, the synthetic recipe of Ag_{16} and Ag_{32} was modified by replacing dppe with dppp (1,3-bis(diphenylphosphino)propane). A pair of optically pure enantiomers

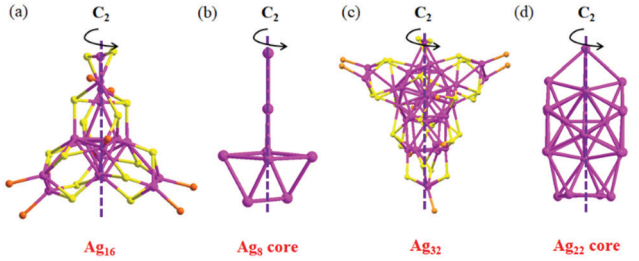

Fig. 9 Core and framework of $Ag_{16}(dppe)_4(SPhF_2)_{14}$ and $Ag_{32}(dppe)_5(SPhCF_3)_{24}$ NCs. Adapted with permission from ref. 27. Copyright 2018, American Chemical Society.

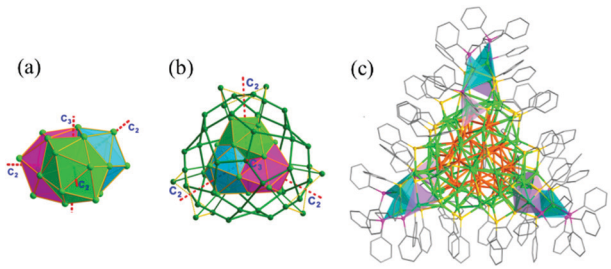

Fig. 10 Core, shell and overall structures of $Ag_{78}(dppp)_6(SPhCF_3)_{42}$. Adapted with permission from ref. 82. Copyright 2017, American Chemical Society.

$Ag_{78}(dppp)_6(SPhCF_3)_{42}$ (R/S-Ag_{78}) were synthesized.[81] The molecular architecture of the R/S-Ag_{78} NCs can be described as a $Ag@Ag_{21}@Ag_{44}@A_{g12}(dppp)_6(SPhCF_3)_{24}(SPhCF_3)_{18}$ core–shell structure (Fig. 10). The $Ag@Ag_{21}$ kernel displays D_3 symmetry and can be described as three mutually inter penetrating icosahedra. The 3-fold axis and three 2-fold axes pass through the center Ag atoms. The $Ag@Ag_{21}$ kernel is encapsulated in a Ag_{44} shell whose structure can be rationalized. The predetermined chirality in the Ag_{78} cluster originates in the chiral arrangement of the surface-protecting units.

Two multi-ligand-protected chiral Ag NCs, $Ag_{32}(dppm)_5(SAdm)_{13}Cl_8$ and $Ag_{45}(dppm)_4(S^tBu)_{16}Br_{12}$, have been synthesized and structurally characterized (Fig. 11).[82] Ag_{32} possesses an achiral Ag_{13} icosahedral kernel, and Ag_{45} also has an achiral core of 23 Ag atoms, but the cores are protected by chiral shells, $Ag_{19}S_{13}C_{l8}P_{10}$ and $Ag_{22}S_{16}P_8Br_{12}$, respectively. It is interesting to note that the coplanar fusion of Ag_{13} units into Ag_{23} constitutes the metal core of the Ag_{45} nanocluster.

Remarkably, the asymmetric distribution of the three types of ligands (thiolate, phosphine, and halogen) on the cluster surface induces chirality that can transfer from the ligand shell to the inner metal core, thereby resulting in an intrinsic chiral structure.

Very recently, Chen *et al.* discovered a new chiral crystal structure of the $Ag_{33}(SCH_2CH_2Ph)_{24}(PPh_3)_4$ NC (Fig. 12).[83] The Ag_{33} nanocluster contains a Ag_{13} icosahedral core and a chiral shell of $Ag_{20}S_{24}P_4$ composed of –SR–Ag–SR– motifs and –Ag–P terminals. $Pd(PPh_3)_4$ played a crucial role in the formation of Ag_{33} but not by replacing silver atoms to form alloys.

The shell-by-shell mode is the most common growth mode for nanoparticles, as reflected in different-size spherical nanoparticles.

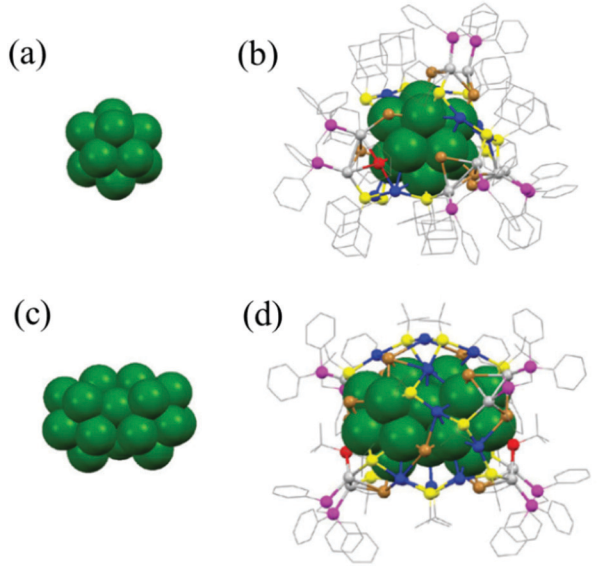

Fig. 11 Core and overall structures of $Ag_{32}(dppm)_5(SAdm)_{13}Cl_8$ and $Ag_{45}(dppm)_4(S^tBu)_{16}Br_{12}$ NCs. Adapted with permission from ref. 81. Copyright 2017, Royal Society of Chemistry.

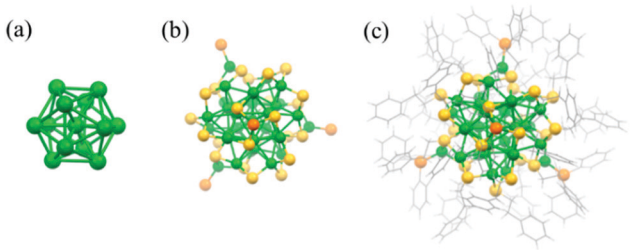

Fig. 12 Core, shell and framework of $Ag_{33}(SCH_2CH_2Ph)_{24}(PPh_3)_4$. Adapted with permission from ref. 83. Copyright 2019, American Chemical Society.

This growth mode allows the isotropic three-dimensional expansion of the particle size and is expected to apply to the structures of giant nanoclusters. Indeed, this mode has been observed in many metal NCs.[6,61] The Zheng and Jin groups solved the crystal structures of a series of plasmonic twinned silver nanoclusters, such as $Ag_{136}(SPh^tBu)_{64}Cl_3Ag_{0.45}$,[84] $Ag_{141}X_{12}(SAdm)_{40}$ (X = Cl, Br, I and SAdm = 1-adamantanethiolate),[85] $Ag_{146}Br_2(SPh^iPr)_{80}$,[86] $Ag_{206}(SCy)_{68}F_2Cl_2$ (Cy: cyclohexanethiolate),[87] and $Ag_{374}(SPh^tBu)_{113}Br_2Cl_2$,[84] which can be described as 5-fold twinned cores enclosed within related structurally distinctive Ag–SR complex shells (Fig. 13).

These large nanoclusters follow the shell-by-shell growth mode, in which a Ag_7 or Ag_{19} innermost kernel and corresponding growth modes have been observed. For the Ag_7-kernel based nanoclusters, $Ag_{146}Br_2(SPh^iPr)_{80}$ can be dissected into Ag_7 (kernel)@Ag_{32} (1st shell)@Ag_{12} (2nd shell)$Ag_{95}Br_2(SPh^iPr)_{80}$[86] and $Ag_{206}(SR)_{68}F_2Cl_2$ follows a Ag_7 (kernel)@Ag_{32} (1st shell)@Ag_{77} (2nd shell)@$Ag_{90}(SCy)_{68}F_2Cl_2$ (motif shell) configuration.[87]

For the Ag_{19}-kernel based nanoclusters, $Ag_{141}(SAdm)_{40}(Cl/Br/I)_{12}$ displays a Ag_{19} (kernel)@Ag_{52} (1st shell)@$Ag_{70}(SAdm)_{68}F_2Cl_2$ (motif shell) three-shell configuration[85] and

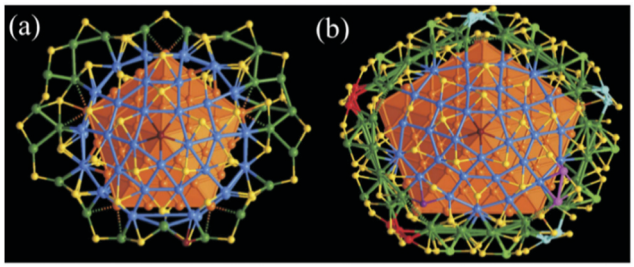

Fig. 13 (a) The shell of Ag_{136} with the bowl-like half J73 related $[Ag_{30}(SPh^tBu)_{15}Cl]$ caps highlighted in blue; and (b) the shell of Ag_{374} with key structure elements highlighted in different colors. Adapted with permission from ref. 84. Copyright 2016 Nature Publishing Group.

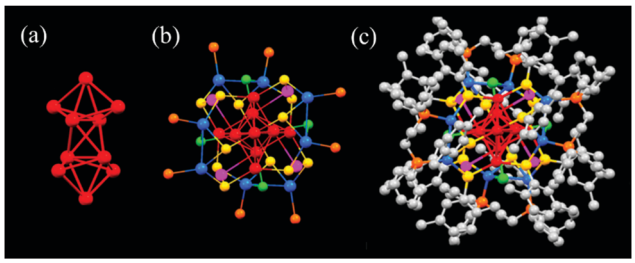

Fig. 14 Core, shell and overall structures of $Ag_{22}(dppe)_4(2,5\text{-}DMBT)_{12}Cl_4$. Adapted with permission from ref. 89. Copyright 2019, American Chemical Society.

$Ag_{210}/_{211}(SPh^iPr)_{71}(PPh_3)_{5/6}Cl$ exhibits a Ag_{19} (kernel)@Ag_{52} (1st shell)@Ag_{45} (2nd shell)@$Ag_{89}(SPh^iPr)_{71}Cl$&(Ag-$PPh_3)_{5/6}$ (motif shell) four-shell configuration.[88]

Unlike the shell-by-shell growth mode in larger metal NCs, many smaller structures have been found to be assembled from small polyhedrons.[6] For instance, the structure of $Ag_{22}(dppe)_4(2,5\text{-}DMBT)_{12}Cl_4$ exhibits a Ag_{10} kernel, which is composed of two Ag_5 units having distorted trigonal bipyramidal geometry (Fig. 14). The Ag_{10} core is protected by a $Ag_{12}(dppe)_4(2,5\text{-}DMBT)_{12}Cl_4$ shell, which is formed by four Ag_2SP_2Cl and four AgS_2 staple motifs.[89] The Ag_{22} cluster exhibits crystallization-enhanced PL.

3.2. Alkynyl-protected Ag CNs

Beyond thiolate ligands, the alkynyl ligand has been employed for the synthesis of a number of coinage metal clusters.[90–92] Recently, some alkynyl-protected Ag NCs have been identified, and they exhibit good stability and crystallizability. For example, Zhang *et al.* and Xie *et al.* exhibited the structures of two all alkynyl-protected Ag NCs, $Ag_{74}(PhC{\equiv}C)_{44}$ and $Ag_{51}(^tBuC{\equiv}C)_{32}$, respectively.[35,36] Their crystal structures both contain three-shell structures. The crystal structure of Ag_{74} possesses a Ag_4 tetrahedron inner core, which is surrounded by the second Ag_{22} shell (Fig. 15).[35] The outermost shell consists of 48 Ag atoms that are enclosed into 12 pentagons and 56 triangles. However, when the phenylacetylene is replaced by *tert*-butylethynide, the Ag_{51} NC is prepared. The crystal structure of Ag_{51} displays a Ag@Ag_{14}@Ag_{36} three shell structure, which is capped by 32 *tert*-butylethynide ligands on the surface (Fig. 16).[36]

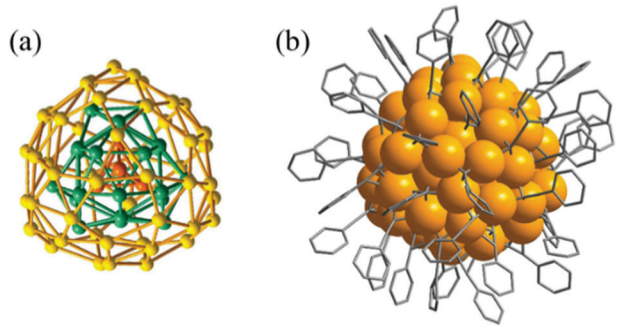

Fig. 15 (a) The Ag_{74} core; and (b) overall structure of $Ag_{74}(PhC{\equiv}C)_{44}$. Adapted with permission from ref. 35. Copyright 2017, American Chemical Society.

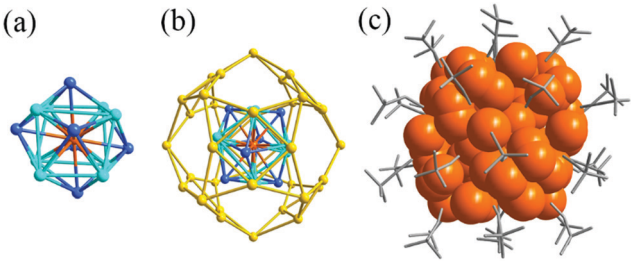

Fig. 16 (a) The Ag@Ag_{14} core; (b) the structure of the Ag@Ag_{14}@Ag_{36} shell; and (c) overall structure of $Ag_{51}(^tBuC{\equiv}C)_{32}$. Adapted with permission from ref. 36. Copyright 2018, Royal Society of Chemistry.

Aside from all alkynyl-protected Ag NCs, alkynyl and auxiliary ligand co-protected Ag NCs have been obtained. In 2017, Wang *et al.* reported two Ag NCs, $Ag_{19}(dppm)_3(PhC{\equiv}C)_{14}^+$ and $Ag_{25}(dpppe)_3(MeOPhC{\equiv}C)_{20}$ (dpppe: 1,5-bis(diphenylphosphino)pentane), which are protected by both alkynyl and phosphine ligands (Fig. 17).[93] They have D_{3h} symmetry with a centered anticuboctahedral Ag_{13} kernel extended by three Ag_2 motifs and three tetrahedral Ag_4 motifs, respectively. Later, they obtained two Ag NCs containing the protection of thiacalixarenes, $Ag_{34}(BTCA)_3(^tBuC{\equiv}C)_9(tfa)_4(CH_3OH)_3$ and $Ag_{35}(H_2BTCA)_2(BTCA)(^tBuC{\equiv}C)_{16}$ (H_4BTCA: 4-*tert*-butylthiacalix[4]arene and tfa: trifluoroacetate).[94,95] The Ag_{34} and Ag_{35} NCs have a centered icosahedral Ag@Ag_{12} kernel that is surrounded by 21 and 22 peripheral silver atoms (Fig. 18), respectively. Surrounding

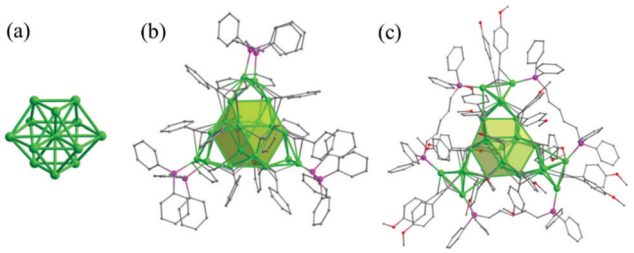

Fig. 17 (a) The Ag_{13} anticuboctahedron kernel; and (b and c) overall structures of $Ag_{19}(dppm)_3(PhC{\equiv}C)_{14}$ and $Ag_{25}(dpppe)_3(MeOPhC{\equiv}C)_{20}$. Adapted with permission from ref. 93. Copyright 2017, Royal Society of Chemistry.

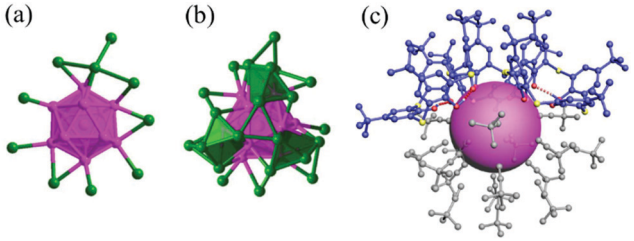

Fig. 18 X-ray structure of $Ag_{35}(H_2BTCA)_2(BTCA)(^tBuC{\equiv}C)_{16}$. (a) Position of 10 peripheral Ag atoms (green) held by thiacalixarene ligands onto the Ag_{13} core (pink); (b) position of 12 peripheral Ag atoms (green, triangular prisms) capped by alkynyl ligands; and (c) side views of the position of surface ligands with respect to the Ag_{35} core. Adapted with permission from ref. 95. Copyright 2015, American Association for the Advancement of Science.

protection for Ag_{35} is provided by three thiacalixarene ligands and 16 alkynyl ligands, while Ag_{34} is protected by four kinds of ligands, including three BTCA, nine alkynyl ligands, four tfa, and three methanol solvent ligands.

Very recently, Wang *et al.* solved the crystal structure of a large alkynyl and halide protected silver NC, $(C_7H_{17}ClN)_3[Ag_{112}Cl_6(ArC{\equiv}C)_{51}]$.[96] The cluster exhibits a four concentric core–shell structure $Ag_{13}@Ag_{42}@Ag_{48}@Ag_9$, and four types of alkynyl–Ag binding modes are observed. Chloride is found to be critical for the stabilization and formation of the Ag NC. Another interesting case is $Ag_{48}(^tBuC{\equiv}C)_{20}(CrO_4)_7$, which is co-capped by CrO_4^{2-} and $^tBuC{\equiv}C^-$ ligands.[97] The pseudo-5-fold symmetric metal skeleton of Ag_{48} shows a core–shell structure composed of a Ag_{23} cylinder encircled by an outer Ag_{25} shell (Fig. 19). The involvement of both organic and inorganic protection is a new path for synthesizing Ag NCs and controlling the formation and structure.

Another interesting case is $Ag_{48}(^tBuC{\equiv}C)_{20}(CrO_4)_7$, which is co-capped by CrO_4^{2-} and $^tBuC{\equiv}C^-$ ligands.[97] The pseudo-5-fold symmetric metal skeleton of Ag_{48} shows a core–shell structure composed of a Ag_{23} cylinder encircled by an outer Ag_{25} shell (Fig. 19). The involvement of both organic and inorganic protection is a new path for synthesizing Ag NCs and controlling the formation and structure.

3.3. Other ligand-protected Ag NCs

It is an effective strategy to obtain new functional metal nanoclusters by using ligands beyond the conventional ones.

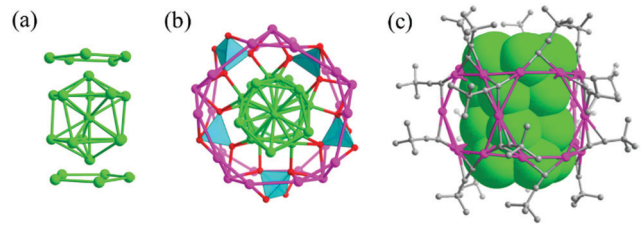

Fig. 19 X-ray structure of $Ag_{48}(^tBuC{\equiv}C)_{20}(CrO_4)_7$. (a) Formation of the Ag_{25} shell by capping two silver pentagons on the Ag_{13} Ino decahedron on the top and bottom; (b) top view of the coordination of five equatorial CrO_4^{2-} anions linking the Ag_{23} cylinder and Ag_{25} shell; and (c) side view of the Ag_{23} cylinder encircled by the outer $[Ag_{25}(^tBuC{\equiv}C)_{20}]$ shell. Adapted with permission from ref. 97. Copyright 2019, American Chemical Society.

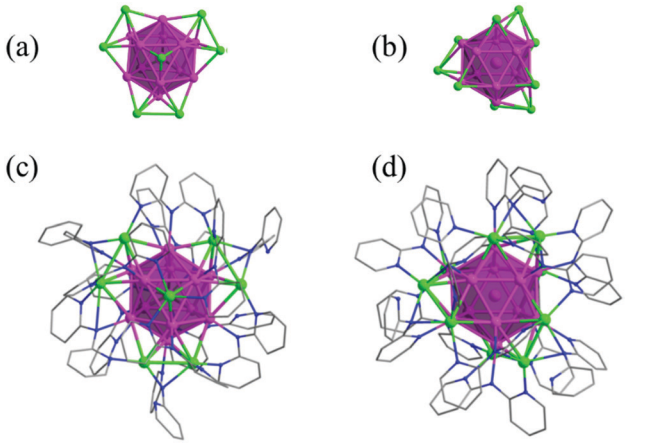

Fig. 20 View of the Ag_{21} kernel (a) and the Ag_{22} kernel (b); and total structures of $A_{g21}(dpa)_{12}$ (c) and $Ag_{22}(dpa)_{12}$ (d) showing the Ag_{13} polyhedron. Adapted with permission from ref. 101. Copyright 2019, Nature Publishing Group.

For example, Liu *et al.* successfully synthesized and determined the structures of $Ag_{20}\{E_2P(OR)_2\}_{12}$ and $Ag_{21}\{E_2P(O^iPr)_2\}_{12}$ (E = S, Se).[98–100] The Ag_{20} and Ag_{21} NCs have a Ag-centered Ag_{13} icosahedral kernel with 7 and 8 capping Ag atoms and 12 dichalcogeno ligands.

Recently, Wang *et al.* reported two homoleptic amido-protected Ag NCs $Ag_{21}(dpa)_{12}$ and $Ag_{22}(dpa)_{12}$ (dpa: dipyridylamido).[101] The Ag_{21} and Ag_{22} NCs consist of a centered-icosahedron Ag_{13} core wrapped by 12 dpa ligands (Fig. 20). The flexible arrangement of the N donors in dpa facilitates the solvent-triggered reversible interconversion between Ag_{21} and Ag_{22} due to their very different solubility.

The Wang group successfully prepared and characterized a Ag NC protected by phosphine and halide, $Ag_{15}(Ntriphos)_4Cl_4$ (N-triphos: tris((diphenylphosphino)methyl)amine).[102] The Ag_{15} cluster has a hexacapped body-centered cubic framework which is consolidated by four tripodal N-triphos ligands, in which one Ag atom occupies the center of the Ag_8 cube, while the six square faces of this Ag_8 cube are capped respectively by one Ag atom (Fig. 21). Our group recently reported three oxometalate and phosphine ligand co-protected Ag NCs, $Ag_{28}(dppb)_6(MoO_4)_4$

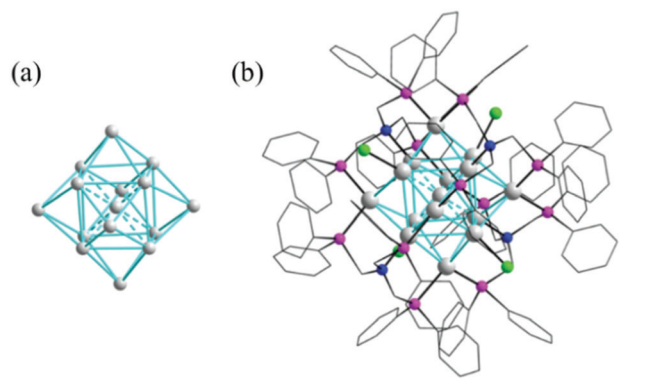

Fig. 21 (a) The core of Ag_{15} in a hexacapped bcc arrangement; and (b) X-ray structure of $[Ag_{15}(Ntriphos)_4(Cl_4)]^{3+}$. Adapted with permission from ref. 102. Copyright 2017, Royal Society of Chemistry.

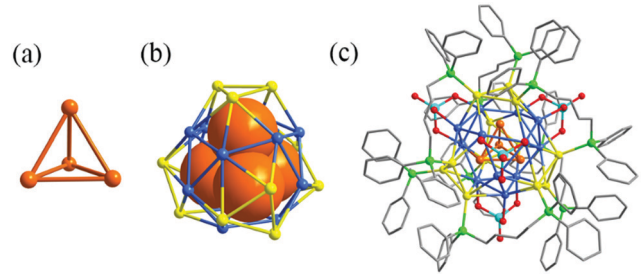

Fig. 22 (a) View of the Ag_4 inner core; (b) the structure of the two-shell $Ag_4@Ag_{24}$; and (c) total structure of $Ag_{28}(dppb)_6(MoO_4)_4$. Adapted with permission from ref. 103. Copyright 2020, Royal Society of Chemistry.

(dppb: 1,4-bis(diphenylphosphino)butane), $Ag_{28}(dppb)_6(WO_4)_4$ and $Ag_{32}(dppb)_{12}(MoO_4)_4(NO_3)_4$.[103] Each cluster comprises a double shell $Ag_4@Ag_{24}$ core covered by 4 oxometalates (Fig. 22). Two similar Ag_{28} cores of our clusters are observed in the $Cu_{12}Ag_{28}(2,4\text{-DCBT})_{24}$ and $Cd_{12}Ag_{32}(SePh)_{36}$ clusters,[104,105] however with vividly different metal and ligand compositions, electronic charges, and surface structures.

In 2019, the Suzuki group prepared a unique ultrastable Ag NC with a C-shaped $\{Si_2W_{18}\}$ building unit (Fig. 23).[106] The $Ag_{27}(Si_2W_{18}O_{66})_3$ cluster was assigned to five octahedral $\{Ag_6\}$ clusters and three bridging Ag atoms, and it was surrounded by C-shaped $\{Si_2W_{18}\}$ through direct Ag–O–W bonds. Recently, Sun *et al.* also reported a series of silver NC based POMs, such as $Ag_{10}@(Mo_7O_{26})_2@Ag_{70}(MoO_4)_2(S^iPr)_{36}(CF_3SO_3)_{16}(DMF)_6$, $Ag_{10}@(MoO_4)_7@Ag_{60}(SPh^tBu)_{33}(mbc)_{18}(DMF)(H_2O)_2$, and $Ag_6@(MoO_4)_7@Ag_{56}(MoO_4)_2(S^iPr)_{28}(CF_3SO_3)_{14}(DMF)_4$.[42,107–109] These large Ag NCs follow the shell-by-shell growth mode, in which a Ag_6 or Ag_{10} innermost kernel and corresponding growth modes have been observed. For example, in the innermost region of $Ag_{10}@(Mo_7O_{26})_2@Ag_{70}(MoO_4)_2(S^iPr)_{36}(CF_3SO_3)_{16}(DMF)_6$, an unusual FCC-structured Ag_{10} nanocluster is locked by a pair of $Mo_7O_{26}^{10-}$ anions to form an inner $Ag_{10}@(Mo_7O_{26})_2$ core which acts as a template to support the outer Ag_{70} nanocluster to form a final three-shell $Ag_{10}@(Mo_7O_{26})_2@Ag_{70}$ nanocluster (Fig. 24).

In contrast to other ligand protected Ag NCs, DNA templated Ag NCs (DNA-Ag NCs) have received much interest, attributable to the photophysical properties including high quantum yield, excellent brightness, photostability, and tunable emission colors from visible to near IR.[110–118] The structures and optical properties of DNA-Ag NCs are regulated by the sequences or

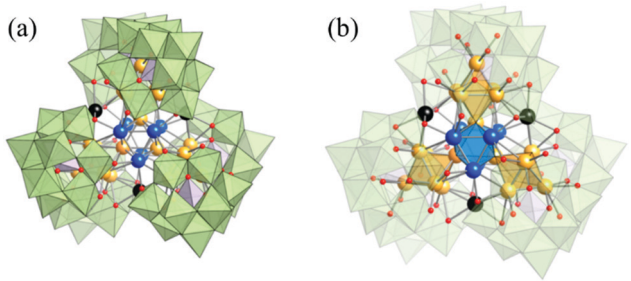

Fig. 23 X-ray structure of $Ag_{27}(Si_2W_{18}O_{66})_3$. Adapted with permission from ref. 106. Copyright 2019, American Chemical Society.

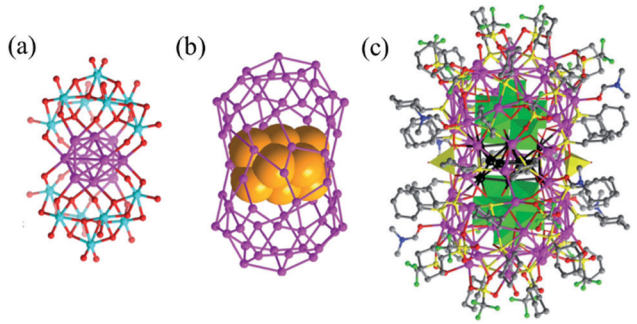

Fig. 24 (a) The Ag_{10} bioctahedron locked by a pair of $Mo_7O_{26}^{10-}$ anions; (b) the Ag_{10} bioctahedron (claybank space-filling balls) residing in the Ag_{70} shell; and (c) overall structure of $Ag_{10}@(Mo_7O_{26})_2@Ag_{70}(MoO_4)_2(S^iPr)_{36}(CF_3SO_3)_{16}(DMF)_6$. Adapted with permission from ref. 107. Copyright 2019, Royal Society of Chemistry.

secondary structures of DNA scaffolds that possess different binding affinities to Ag NCs. The first example of DNA-Ag NCs was discovered by Dickson and co-workers in 2004,[119] where a 12-base scaffold of 5′-AGGTCGCCGCCC-3′ was employed as the template to direct the assembly of silver ions, and then reduced by $NaBH_4$ to form Ag NCs in aqueous solution at room temperature. By choosing DNA templates with various sequences and lengths, many types of fluorescent DNA-Ag NCs were prepared.[110–123] Mass spectrometry reveals that the sequence and length of DNA scaffolds could play an important role in determining the size of Ag NCs. In addition to the size, the DNA conformation and the oxidation state of Ag NCs are other factors that modulate the structures and optical properties.

The secondary structure of DNA scaffolds has also important influences on the structure and optical properties of DNA-Ag NCs. Secondary structures such as hairpin, i-motif and G-quadruplex have been made in creating DNA-Ag NCs. For example, DNA-Ag NCs can be prepared by using hairpins with a C-loop of 3 to 12 cytosines, which contained different numbers of silver atoms and showed different fluorescence.[120–122]

Li *et al.* synthesized fluorescent DNA-Ag NCs with i-motif DNA, and such NCs display an emission wavelength range over green to NIR.[123] By using a G-quadruplex DNA sequence, Wang *et al.* synthesized dual-emissive DNA-Ag NCs possessing high thermo-stability.[124] To better understand the properties and applications of DNA-Ag NCs, readers are also recommended to refer to recent reviews.[125–134]

4. Optical properties of Ag NCs

4.1. UV-vis absorption

Surface plasmon resonance (SPR) is the most prominent feature in the UV-vis absorption spectra of Ag NPs due to their distinct optical absorption.[135–138] The SPR peak of Ag NPs is typically located at about 400 nm. In contrast, Ag NCs generally show several distinct absorption peaks in the UV-vis region. The optical absorptions of Ag NCs and Ag NPs are distinctively different, with different origins and different peak locations. Such data can be used to confirm the successful synthesis of Ag

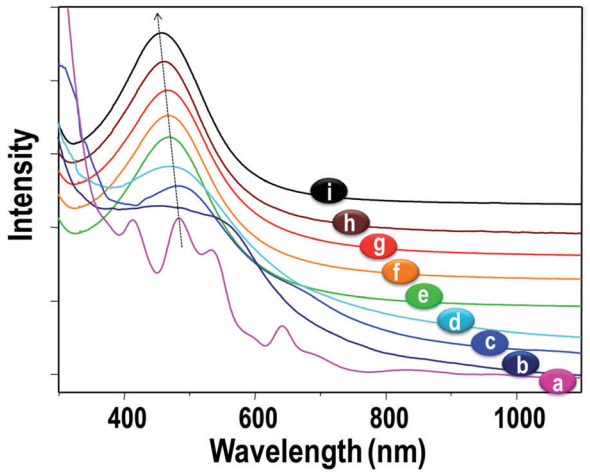

Fig. 25 UV-vis absorption spectra of thiol-protected Ag_{44} [a], Ag_{55} [b], $Ag_{\sim 75}$ [c], $Ag_{\sim 114}$ [d], Ag_{152} [e], $Ag_{\sim 202}$ [f], $Ag_{\sim 423}$ [g], $Ag_{\sim 530}$ [h] and Ag NPs [i]. Reproduced with permission from ref. 140. Copyright 2014, Royal Society of Chemistry.

NCs and the transformation of small Ag NCs into large plasmonic Ag NPs.

The surface ligands and cluster size can affect the optical absorption of Ag NCs (Table S2, ESI†). For example, thiol-protected Ag_{2-8} NCs showed discrete absorption peaks in their UV-vis absorption spectra.[139] The UV-vis spectra of thiol-protected Ag NCs, such as Ag_{44}(4-FTP)$_{30}$, $Ag_{55}(PET)_{31}$, $Ag_{75}(PET)_{40}$, $Ag_{114}(PET)_{46}$, $Ag_{152}(PET)_{60}$, $Ag_{202}(BBS)_{70}$, $Ag_{423}(PET)_{105}$, and $Ag_{530}(PET)_{100}$, show multiple features up to Ag_{114} and, from Ag_{152} onwards, only one absorption peak at 460 nm (Fig. 25).

The change of the protecting ligands and cluster size, which affect the behavior in the excited state, results in an alteration of the electronic transition.[140] Insight into the modulation of the PL properties and the relaxation from the excited state is provided in the following sections.

4.2. Photoluminescence

PL is amongst the most intriguing and fascinating properties of nanomaterials due to the scope in diverse applications. Ag NCs excited from the ground state release extra energy before returning back to the ground state, which gives rise to PL. However, Ag NCs normally display low quantum yield (QY), and some fundamental issues related to the PL properties of Ag NCs are still indistinct. The PL of Ag NCs can be dictated by the cluster size, protecting ligand, and heterometal atom. Moreover, the valence electron count, oxidation state of the metal, crystal structure, temperature, and pH are crucial to regulate the PL behavior.[31,32]

4.2.1. Influence of peripheral ligands. In 2001, Dickson[141] reported bright PL from individual Ag NCs, which accelerated research into metal NCs stabilized with various ligands such as thiols, phosphines, alkynyls or their combination. These peripheral ligands have been proved to have a profound influence on the PL of NCs. With the revelation of different PL behavior in Ag NCs, the effect of the functional groups in the capping ligands has been realized. For example, the $C_{12}H_6O_2NCH_2CO_2^-$ ligand Ag_{20} nanocluster showed green emission around 513 nm with a high PL QY of 6.36% at room temperature. However, the fluorescence was completely quenched in terms of the substitution of the $C_{12}H_6O_2NCH_2CO_2^-$ ligand with NO_3^- or other ligands.[142] The NIR emission of $[Ag_{29}(BDT)_{12}(PPh_3)_4]^{3-}$ NCs increases 30 fold when monophosphine ligands are replaced by diphosphines with increased chain length.[143]

The ligand effect on the PL of a Ag_{62} nanocluster template has been investigated. The tetracationic silver nanocluster $[Ag_{62}S_{13}(S^tBu)_{32}]^{4+}$ (Ag-QDs) has been reported with intense red emission at 613 nm (solution) and 621 nm (solid state).[65] Later, Zhu *et al.* reported the crystal structure of $[Ag_{62}S_{12}(S^tBu)_{32}]^{2+}$ (Ag-NCs),[64] which can be regarded as $[Ag_{62}S_{13}(S^tBu)_{32}]^{4+}$ lacking the innermost S ligand. The PL intensity of the Ag-NCs was much weaker than that of the Ag-QDs due to the difference in the valence electron count. The 4 free valence electrons in the Ag-NCs cause luminescence quenching as the LMCT process (ligand-to-metal charge transfer) gets hindered, while the Ag-QDs exhibit intense PL owing to the absence of free valence electrons. Interestingly, the Ag-QDs could be electrochemically reduced into Ag-NCs, *via* an intermediate NC, Ag-inter.[66] Though the structural integrity of the parent Ag_{62} remains unaltered, the PL intensity of the Ag-inter displayed a 2-fold enhancement relative to the Ag-NCs, and it was still far below the intensity of the Ag-QDs (Fig. 26).

4.2.2. Tuning of the emission with the core size. Etching of silver NPs at the water–toluene interface with MSA ends up with a crude mixture of Ag_7 and Ag_8 NCs. After separation by gel electrophoresis, the Ag_7 NCs display bluish green emission at 440 nm while weak red emission at 650 nm is observed in the Ag_8 NCs.[49] In 2003, Zheng *et al.* reported the $Ag_{14}(SC_6H_3F_2)_{12}(PPh_3)_8$ NC with yellow luminescence.[68] The comparatively large NCs, $Ag_{16}(dppe)_4(SC_6H_3F_2)_{14}$ and $Ag_{32}(dppe)_5(SC_6H_3CF_3)_{24}$, exhibit only a prominent emission peak at 440 nm.[80] More information about the PL of Ag NCs with various core sizes is given in Table S2 (ESI†).

4.2.3. Influence of the doped atoms. Doping with foreign metal atoms in Ag NCs has been proved to be an effective method for the modulation of the geometric and electronic structures, and thus could be used to tune the PL (Fig. 27).

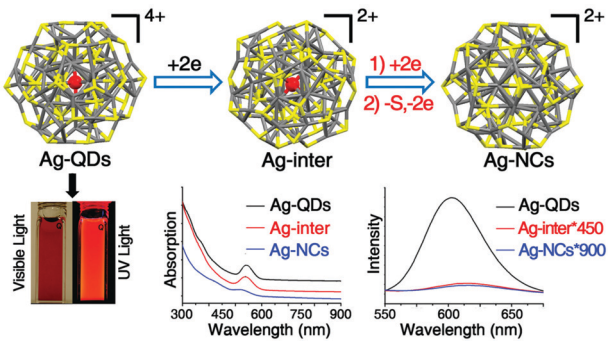

Fig. 26 Schematic illustration of the structural transformation on the basis of a Ag_{62} nanocluster template from Ag-QDs to Ag-inter, and then to Ag-NCs; (bottom-left) digital photographs of Ag-QDs under visible and UV light; and (bottom-middle and -right) UV-vis and PL spectra of Ag-QDs, Ag-inter, and Ag-NCs. Reproduced with permission from ref. 31. Copyright 2019, Royal Society of Chemistry.

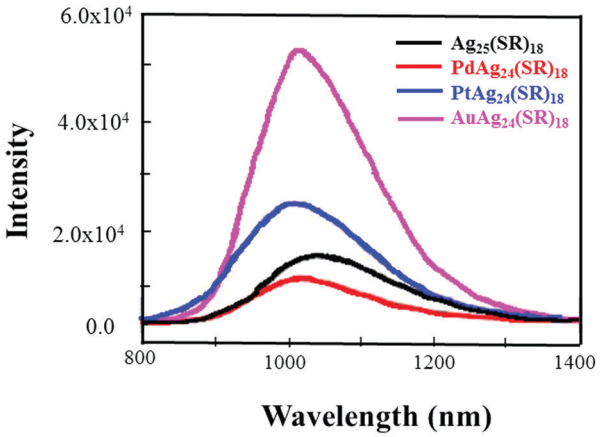

Fig. 27 PL spectra of $MAg_{24}(SR)_{18}$ (M = Ag/Pd/Pt/Au) NCs in the crystal state. Reproduced with permission from ref. 148. Copyright 2017, American Chemical Society.

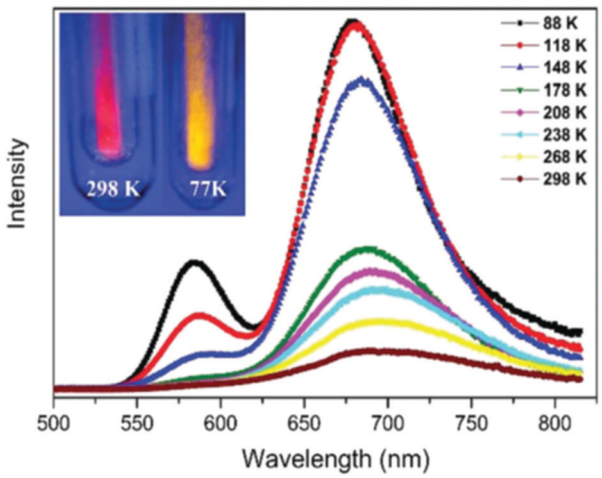

Fig. 29 Effect of temperature on the PL of Ag_{18} in the solid state at 440 nm excitation. Adapted with permission from ref. 130. Copyright 2017, Royal Society of Chemistry.

The optical, electrochemical, and catalytic properties of metal NCs $M_1Ag_{24}(SR)_{18}$ (M = Ag, Au, Pd, Pt) have been systematically characterized.[23,144–148] For example, Bootharaju *et al.* demonstrated the PL property enhancement of $Ag_{25}(SPhMe_2)_{18}$ doped with Pd or Au. Due to the stabilization of the charges in the LUMO of the alloy cluster akin to $Au_{25-n}Ag_n$ NCs, the luminescence of the Ag_{25} cluster is enhanced by a factor of 25 upon doping with gold atoms.[144] Wu *et al.* investigated the PL property of $M@Ag_{24}(DMBT)_{18}$ (M = Ag, Pd, Pt, Au) in both crystal and solution phases.[148] A blue shift of the PL with the doping of $Ag_{25}(DMBT)_{18}$ by Pd/Pt/Au heteroatoms is observed. The sequence of the PL intensity $PdAg_{24}(DMBT)_{18} < Ag_{25}(DMBT)_{18} < PtAg_{24}(DMBT)_{18} < AuAg_{24}(DMBT)_{18}$ is exactly related to the electron affinity of the core atom (Fig. 28).

$Ag_{29}(S_2R)_{12}(PPh_3)_4$ is another fluorescent Ag NC which has been studied in the context of doping. The PL characteristic of the $Ag_{29}(S_2R)_{12}(PPh_3)_4$ NC has been tuned by doping such a NC with Au/Pt ions. The introduction of the Au or Pt heteroatoms improves the PL intensity relative to the homo-silver Ag_{29} NC. Bootharaju *et al.* reported the enhancement of the PL intensity in doped $PtAg_{28}(BDT)_{12}(TPP)_4$ compared to homo-silver Ag_{29}NCs.[149] Soldan *et al.* prepared metal NCs $Ag_{29-x}Au_x(BDT)_{12}(TPP)_4$ and demonstrated that the emission maxima are red shifted from 658 nm (10% Au) to 668 nm (40% Au) with an increase in the Au concentration (Fig. 28).[150]

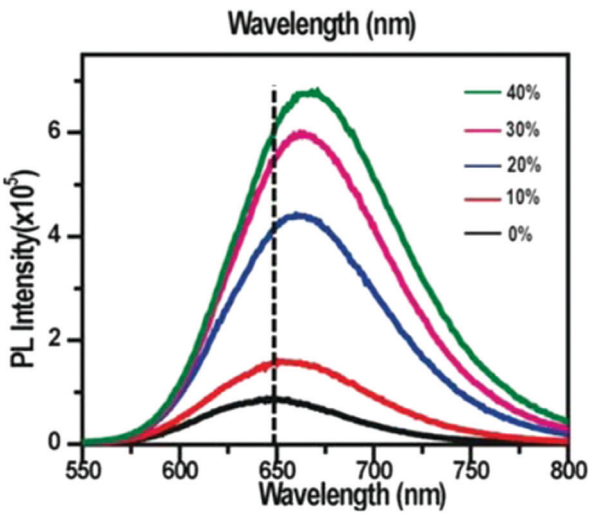

Fig. 28 PL spectra of Ag_{29} and Au doped Ag_{29} NCs with different amounts (mmol%) of Au. The inset shows digital photographs under a UV lamp (365 nm). Adapted with permission from ref. 150. Copyright 2016, John Wiley & Sons, Inc.

4.2.4. Influence of the surrounding environment. Apart from the core size and protecting ligand, the PL behavior of Ag NCs is altered by different external factors such as temperature, solvent, pH *etc.* For example, the temperature-dependent PL properties of a series of Ag NCs were reported by the Sun group.[107,151–159] Some Ag NCs exhibited higher PL intensities at low temperature, but the emission wavelengths were little changed. However, the emission maximum of the Ag_{180} NC shifts from 723 nm to 623 nm with lowering of the temperature from 293 K to 93 K.[131] The Ag_{18} NC displays an emission wavelength change from red emission (700 nm) to yellow (550 nm) when the temperature of the Ag_{18} NC was reduced (Fig. 29).[155] Of note, PL intensity enhancement and emission wavelength shifts for nanocluster-based networks have also been researched by the Zang group.[72,160–165]

Solvents can also influence the PL properties of NCs, although to a lesser degree than that seen in metal complexes. Silver NCs, being composed of diverse functional groups in the surface ligand, often display solvent specific optical behavior. The nature of the solvent (polarity, protic or aprotic, coordinating or non-coordinating) controls the electronic properties, which eventually influence the emission of Ag NCs.[92,101,148] Xie *et al.* evaluated the solvatochromism of the $Ag_{51}(^tBuC{\equiv}C)_{32}$ NC.[92] As the solvent polarity increased from less polar dichloromethane to highly polar methanol, the emission peaks of Ag_{51} are gradually red-shifted from 436 to 656 nm, exhibiting a remarkable bathochromic effect (Fig. 30).

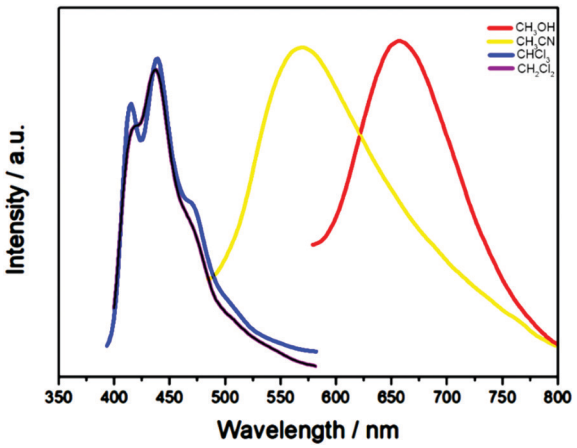

Fig. 30 Emission bands of Ag_{51} in solvents of varying polarity, CH_2Cl_2 (purple line), $CHCl_3$ (blue line), CH_3CN (yellow line) and CH_3OH (red line). Adapted with permission from ref. 92. Copyright 2018, Royal Society of Chemistry.

Ag NCs feature tunable luminescence properties, photostability and a biocompatible nature, and have enthralled the scientific community for their applicability in versatile applications such as optoelectronics, catalysis, bio-sensing, and bio-imaging.[6,7,12,13,29,31] More studies are required to explore new applications of Ag NCs. Further development of multi-photon excitation microscopy in Ag NCs calls for more efforts. More Ag NCs with visible range absorption still need to be developed in photovoltaic applications. Biological applications such as bio-sensing and bio-imaging demand hydrophilic Ag NCs with very high PLQY, while catalytic applications need structurally precise Ag NCs.

5. Conclusions

We have summarized significant advances in the field of Ag NCs such as synthesis, structure, and PL properties. For instance, a number of efficient synthetic strategies including direct reduction, chemical etching, and ligand exchange have been developed to produce Ag NCs. Some high-resolution analytical techniques have emerged as powerful tools to characterize Ag NCs, including UV-vis, PL, ESI-MS, SC-XRD, *etc.* Such techniques have been used to determine the chemical properties and crystal structures of Ag NCs. The crystal structures of Ag NCs eventually control the electronic transition and physical properties. The PL properties of Ag NCs are modulated by the valence state, electronic structure, functional groups and doping heteroatoms. Some parameters of the surroundings such as temperature and solvent also tune the PL properties of Ag NCs.

However, although we have witnessed remarkable progress in the study of Ag NCs, some challenging issues still remain. For example, efficient synthetic strategies for high-purity Ag NCs in the aqueous phase are still lacking. Strategies for increasing the PL quantum yield and tuning the PL colors of nanoclusters are to be devised. Much more effort is needed to further explore promising luminescent probes for a wide spectrum of bio-imaging and bio-sensing applications.

Conflicts of interest

There are no conflicts to declare.

Acknowledgements

We gratefully acknowledge financial support from the National Natural Science Foundation of China (No. 21771071, 51672093 and 21925104).

Notes and references

1 G. Schmid, Large clusters and colloids. Metals in the embryonic state, *Chem. Rev.*, 1992, **92**, 1709–1727.
2 M.-C. Daniel and D. Astruc, Gold nanoparticles: assembly, supramolecular chemistry, quantum-size-related properties, and applications toward biology, catalysis, and nanotechnology, *Chem. Rev.*, 2004, **104**, 293–346.
3 R. Jin, Quantum sized, thiolate-protected gold nanoclusters, *Nanoscale*, 2010, **2**, 343–362.
4 Y. Lu and W. Chen, Sub-nanometre sized metal clusters: from synthetic challenges to the unique property discoveries, *Chem. Soc. Rev.*, 2012, **41**, 3594–3623.
5 H. Qian, M. Zhu, Z. Wu and R. Jin, Quantum sized gold nanoclusters with atomic precision, *Acc. Chem. Res.*, 2012, **45**, 1470–1479.
6 R. Jin, C. Zeng, M. Zhou and Y. Chen, Atomically precise colloidal metal nanoclusters and nanoparticles: fundamentals and opportunities, *Chem. Rev.*, 2016, **116**, 10346–10413.
7 I. Chakraborty and T. Pradeep, Atomically precise clusters of noble metals: emerging link between atoms and nanoparticles, *Chem. Rev.*, 2017, **117**, 8208–8271.
8 C. M. Aikens, Electronic structure of ligand-passivated gold and silver nanoclusters, *J. Phys. Chem. Lett.*, 2011, **2**, 99–104.
9 N. Goswami, K. Zheng and J. Xie, Bio-NCs-the marriage of ultrasmall metal nanoclusters with biomolecules, *Nanoscale*, 2014, **6**, 13328–13347.
10 A. Fernando, K. L. D. M. Weerawardene, N. V. Karimova and C. M. Aikens, Quantum mechanical studies of large metal, metal oxide, and metal chalcogenide nanoparticles and clusters, *Chem. Rev.*, 2015, **115**, 6112–6216.
11 S. A. Díaz, D. A. Hastman, I. L. Medintz and E. Oh, Understanding energy transfer with luminescent gold nanoclusters: a promising new transduction modality for biorelated applications, *J. Mater. Chem. B*, 2017, **5**, 7907–7926.
12 S. Maity, D. Bain and A. Patra, An overview on the current understanding of the photophysical properties of metal nanoclusters and their potential applications, *Nanoscale*, 2019, **11**, 22685–22723.
13 D. Bain, S. Maity and A. Patra, Opportunities and challenges in energy and electron transfer of nanocluster based hybrid materials and their sensing applications, *Phys. Chem. Chem. Phys.*, 2019, **21**, 5863–5881.
14 Y. Du, H. Sheng, D. Astruc and M. Zhu, Atomically precise noble metal nanoclusters as efficient catalysts: a bridge

between structure and properties, *Chem. Rev.*, 2020, **120**, 526–622.
15 R. Jin, Atomically precise metal nanoclusters: stable sizes and optical properties, *Nanoscale*, 2015, **7**, 1549–1565.
16 M. W. Heaven, A. Dass, P. S. White, K. M. Holt and R. W. Murray, Crystal structure of the gold nanoparticle $[N(C_8H_{17})_4][Au_{25}(SCH_2CH_2Ph)_{18}]$, *J. Am. Chem. Soc.*, 2008, **130**, 3754–3755.
17 M. Zhu, C. M. Aikens, F. J. Hollander, G. C. Schatz and R. Jin, Correlating the crystal structure of a thiol-protected Au_{25} cluster and optical properties, *J. Am. Chem. Soc.*, 2008, **130**, 5883–5885.
18 M. Zhu, W. T. Eckenhoff, T. Pintauer and R. Jin, Conversion of anionic $[Au_{25}(SCH_2CH_2Ph)_{18}]-$ cluster to charge neutral cluster via air oxidation, *J. Phys. Chem. C*, 2008, **112**, 14221–14224.
19 N. K. Chaki, Y. Negishi, H. Tsunoyama, Y. Shichibu and T. Tsukuda, Ubiquitous 8 and 29 kDa gold: alkanethiolate cluster compounds: mass-spectrometric determination of molecular formulas and structural implications, *J. Am. Chem. Soc.*, 2008, **130**, 8608–8610.
20 H. Qian, Y. Zhu and R. Jin, Size-socusing synthesis, optical and electrochemical properties of monodisperse $Au_{38}(SC_2H_4Ph)_{24}$ nanoclusters, *ACS Nano*, 2009, **3**, 3795–3803.
21 H. Qian, W. T. Eckenhoff, Y. Zhu, T. Pintauer and R. Jin, Total structure determination of thiolate-protected Au_{38} nanoparticles, *J. Am. Chem. Soc.*, 2010, **132**, 8280–8281.
22 P. D. Jadzinsky, G. Calero, C. J. Ackerson, D. A. Bushnell and R. D. Kornberg, Structure of a thiol monolayer-protected gold nanoparticle at 1.1 Å resolution, *Science*, 2007, **318**, 430–433.
23 C. P. Joshi, M. S. Bootharaju, M. J. Alhilaly and O. M. Bakr, $[Ag_{25}(SR)_{18}]-$: The ''golden'' silver nanoparticle, *J. Am. Chem. Soc.*, 2015, **137**, 11578–11581.
24 L. G. AbdulHalim, M. S. Bootharaju, Q. Tang, S. Del Gobbo, R. G. AbdulHalim, M. Eddaoudi, D.-E. Jiang and O. M. Bakr, $Ag_{29}(BDT)_{12}(TPP)_4$: a tetravalent nanocluster, *J. Am. Chem. Soc.*, 2015, **137**, 11970–11975.
25 A. Desireddy, B. E. Conn, J. Guo, B. Yoon, R. N. Barnett, B. M. Monahan, K. Kirschbaum, W. P. Griffith, R. L. Whetten, U. Landman and T. P. Bigioni, Ultrastable silver nanoparticles, *Nature*, 2013, **501**, 399–402.
26 H. Yang, Y. Wang, H. Huang, L. Gell, L. Lehtovaara, S. Malola, H. Häkkinen and N. Zheng, All-thiol-stabilized Ag_{44} and $Au_{12}Ag_{32}$ nanoparticles with single-crystal structures, *Nat. Commun.*, 2013, **4**, 2422–2429.
27 J. Yan, B. K. Teo and N. Zheng, Surface chemistry of atomically precise coinage-metal nanoclusters: from structural control to surface reactivity and catalysis, *Acc. Chem. Res.*, 2018, **51**, 3084–3093.
28 T. Udayabhaskararao and T. Pradeep, New protocols for the synthesis of stable Ag and Au nanocluster molecules, *J. Phys. Chem. Lett.*, 2013, **4**, 1553–1564.
29 K. Zheng, X. Yuan, N. Goswami, Q. Zhang and J. Xie, Recent advances in the synthesis, characterization, and biomedical applications of ultrasmall thiolated silver nanoclusters, *RSC Adv.*, 2014, **4**, 60581–60596.
30 J. Yang and R. Jin, New advances in atomically precise silver nanoclusters, *ACS Mater. Lett.*, 2019, **1**, 482–489.
31 X. Kang and M. Zhu, Tailoring the photoluminescence of atomically precise nanoclusters, *Chem. Soc. Rev.*, 2019, **48**, 2422–2457.
32 H. Yu, B. Rao, W. Jiang, S. Yang and M. Zhu, The photoluminescent metal nanoclusters with atomic precision, *Coord. Chem. Rev.*, 2019, **378**, 595–617.
33 Q. Yao, T. Chen, X. Yuan and J. Xie, Toward total synthesis of thiolate-protected metal nanoclusters, *Acc. Chem. Res.*, 2018, **51**, 1338–1348.
34 N. Goswami, Q. Yao, T. Chen and J. Xie, Mechanistic exploration and controlled synthesis of precise thiolate-gold nanoclusters, *Coord. Chem. Rev.*, 2016, **329**, 1–15.
35 M. Qu, H. Li, L.-H. Xie, S.-T. Yan, J.-R. Li, J.-H. Wang, C.-Y. Wei, Y.-W. Wu and X.-M. Zhang, Bidentate phosphine-assisted synthesis of an all-alkynyl-protected Ag_{74} nanocluster, *J. Am. Chem. Soc.*, 2017, **139**, 12346.
36 G.-X. Duan, L. Tian, J.-B. Wen, L.-Y. Li, Y.-P. Xie and X. Lu, An atomically precise all-tert-butylethynide-protected Ag_{51} superatom nanocluster with color tenability, *Nanoscale*, 2018, **10**, 18915–18919.
37 Y. Chen, C. Zeng, D. R. Kauffman and R. Jin, Tuning the magic size of atomically precise gold nanoclusters via isomeric methylbenzenethiols, *Nano Lett.*, 2015, **15**, 3603–3609.
38 M. A. Muhammed, F. Aldeek, G. Palui, L. Trapiella-Alfonso and H. Mattoussi, Growth of in situ functionalized luminescent silver nanoclusters by direct reduction and size focusing, *ACS Nano*, 2012, **6**, 8950–8961.
39 B. Adhikari and A. Banerjee, Facile synthesis of water-soluble fluorescent silver nanoclusters and Hg^{II} sensing, *Chem. Mater.*, 2010, **22**, 4364–4371.
40 Z. Wu, E. Lanni, W. Chen, M. E. Bier, D. Ly and R. Jin, High yield, large scale synthesis of thiolate-protected Ag_7 clusters, *J. Am. Chem. Soc.*, 2009, **131**, 16672–16674.
41 I. Chakraborty, T. Udayabhaskararao and T. Pradeep, High temperature nucleation and growth of glutathione protected $\sim Ag_{75}$ clusters, *Chem. Commun.*, 2012, **48**, 6788–6790.
42 Z. Wang, R. K. Gupta, G.-G. Luo and D. Sun, Design and development of highly efficient light-emitting layers in OLEDs with dimesitylboranes: an updated review, *Chem. Rec.*, 2019, **19**, 1–15.
43 I. Chakraborty, T. Udayabhaskararao, G. K. Deepesh and T. Pradeep, Sunlight mediated synthesis and antibacterial properties of monolayer protected silver clusters, *J. Mater. Chem. B*, 2013, **1**, 4059–4064.
44 T. Zhou, M. Rong, Z. Cai, C. J. Yang and X. Chen, Sonochemical synthesis of highly fluorescent glutathione-stabilized Ag nanoclusters and S^2- sensing, *Nanoscale*, 2012, **4**, 4103–4106.
45 B. S. González, M. Blanco and M. A. López-Quintela, Single step electrochemical synthesis of hydrophilic/hydrophobic Ag_5 and Ag_6 blue luminescent clusters, *Nanoscale*, 2012, **4**, 7632–7635.
46 X. Le Guével, C. Spies, N. Daum, G. Jung and M. Schneider, Highly fluorescent silver nanoclusters stabilized by glutathione:

a promising fluorescent label for bioimaging, *Nano Res.*, 2012, **5**, 379–387.

47 X. Yuan, M. I. Setyawati, A. S. Tan, C. N. Ong, D. T. Leong and J. Xie, Highly luminescent silver nanoclusters with tunable emissions: cyclic reduction-decomposition synthesis and antimicrobial properties, *NPG Asia Mater.*, 2013, **5**, e39.

48 K. V. Mrudula, T. Udayabhaskararao and T. Pradeep, Interfacial synthesis of luminescent 7 kDa silver clusters, *J. Mater. Chem.*, 2009, **19**, 4335–4342.

49 T. Udayabhaskararao and T. Pradeep, Luminescent Ag_7 and Ag_8 clusters by interfacial synthesis, *Angew. Chem., Int. Ed.*, 2010, **49**, 3925–3929.

50 L. Dhanalakshmi, T. Udayabhaskararao and T. Pradeep, Conversion of double layer charge-stabilized Ag@citrate colloids to thiol passivated luminescent quantum clusters, *Chem. Commun.*, 2012, **48**, 859–861.

51 L. G. AbdulHalim, N. Kothalawala, L. Sinatra, A. Dass and O. M. Bakr, Neat and complete: Thiolate-ligand exchange on a silver molecular nanoparticle, *J. Am. Chem. Soc.*, 2014, **136**, 15865–15868.

52 M. S. Bootharaju, V. M. Burlakov, T. M. D. Besong, C. P. Joshi, L. G. AbdulHalim, D. M. Black, R. L. Whetten, A. Goriely and O. M. Bakr, Reversible size control of silver nanoclusters via ligand-exchange, *Chem. Mater.*, 2015, **27**, 4289–4297.

53 M. S. Bootharaju, C. P. Joshi, M. J. Alhilaly and O. M. Bakr, Switching a nanocluster core from hollow to nonhollow, *Chem. Mater.*, 2016, **28**, 3292–3297.

54 E. Khatun, A. Ghosh, D. Ghosh, P. Chakraborty, A. Nag, B. Mondal, S. Chennu and T. Pradeep, $[Ag_{59}(2,5\text{-DCBT})_{32}]^{3}-$: a new cluster and a precursor for three well-known clusters, *Nanoscale*, 2017, **9**, 8240–8248.

55 T. Udayabhaskararao, B. Nataraju and T. Pradeep, Ag_9 quantum cluster through a solid-state route, *J. Am. Chem. Soc.*, 2010, **132**, 16304–16307.

56 T. Udayabhaskararao, M. Bootharaju and T. Pradeep, Thiolate-protected Ag_{32} clusters: mass spectral studies of composition and insights into the Ag-thiolate structure from NMR, *Nanoscale*, 2013, **5**, 9404–9411.

57 I. Chakraborty, A. Govindarajan, J. Erusappan, A. Ghosh, T. Pradeep, B. Yoon, R. L. Whetten and U. Landman, The superstable 25 kDa monolayer protected silver nanoparticle: measurements and interpretation as an icosahedral $Ag_{152}(SCH_2CH_2Ph)_{60}$ cluster, *Nano Lett.*, 2012, **12**, 5861–5866.

58 I. Chakraborty, W. Kurashige, K. Kanehira, L. Gell, H. Häkkinen, Y. Negishi and T. Pradeep, $Ag_{44}(SeR)_{30}$: a hollow cage silver cluster with selenolate protection, *J. Phys. Chem. Lett.*, 2013, **4**, 3351–3355.

59 I. Chakraborty, T. Udayabhaskararao and T. Pradeep, Luminescent sub-nanometer clusters for metal ion sensing: A new direction in nanosensors, *J. Hazard. Mater.*, 2012, **211–212**, 396–403.

60 W. Du, S. Jin, L. Xiong, M. Chen, J. Zhang, X. Zou, Y. Pei, S. Wang and M. Zhu, $Ag_{50}(Dppm)_6(SR)_{30}$ and its homologue $Au_xAg_{50-x}(Dppm)_6(SR)_{30}$ alloy nanocluster: seeded growth, structure determination, and differences in properties, *J. Am. Chem. Soc.*, 2017, **139**, 1618–1624.

61 X. Kang and M. Zhu, Intra-cluster growth meets inter-cluster assembly: the molecular and supramolecular chemistry of atomically precise nanoclusters, *Coord. Chem. Rev.*, 2019, **394**, 1–38.

62 X. Du, J. Chai, S. Yang, Y. Li, T. Higaki, S. Li and R. Jin, Fusion growth patterns in atomically precise metal nanoclusters, *Nanoscale*, 2019, **11**, 19158–19165.

63 T. Higaki, C. Zeng, Y. Chen, E. Hussain and R. Jin, Controlling the crystalline phases (FCC, HCP and BCC) of thiolate-protected gold nanoclusters by ligand-based strategies, *CrystEngComm*, 2016, **18**, 6979–6986.

64 S. Jin, S. Wang, Y. Song, M. Zhou, J. Zhong, J. Zhang, A. Xia, Y. Pei, M. Chen, P. Li and M. Zhu, Crystal structure and optical properties of the $[Ag_{62}S_{12}(SBut)_{32}]^{2+}$ nanocluster with a complete face-centered cubic kernel, *J. Am. Chem. Soc.*, 2014, **136**, 15559–15565.

65 G. Li, Z. Lei and Q.-M. Wang, Luminescent molecular Ag–S nanocluster $[Ag_{62}S_{13}(SBut)_{32}](BF_4)_4$, *J. Am. Chem. Soc.*, 2010, **132**, 17678–17679.

66 S. Jin, S. Wang, L. Xiong, M. Zhou, S. Chen, W. Du, A. Xia, Y. Pei and M. Zhu, Two electron reduction: From quantum dots to metal nanoclusters, *Chem. Mater.*, 2016, **28**, 7905–7911.

67 X. Liu, J. Chen, J. Yuan, Y. Li, J. Li, S. Zhou, C. Yao, L. Liao, S. Zhuang, Y. Zhao, H. Deng, J. Yang and Z. Wu, A silver nanocluster containing interstitial sulfur and unprecedented chemical bonds, *Angew. Chem., Int. Ed.*, 2018, **57**, 11273–11277.

68 H. Yang, J. Lei, B. Wu, Y. Wang, M. Zhou, A. Xia, L. Zheng and N. Zheng, Crystal structure of a luminescent thiolated Ag nanocluster with an octahedral Ag_6^{4+} core, *Chem. Commun.*, 2013, **49**, 300–302.

69 C. Liu, T. Li, H. Abroshan, Z. Li, C. Zhang, H. Kim, G. Li and R. Jin, Chiral Ag_{23} nanocluster with open shell electronic structure and helical face-centered cubic framework, *Nat. Commun.*, 2018, **9**, 744–749.

70 B. K. Teo, H. Yang, J. Yan and N. Zheng, Supercubes, supersquares, and superrods of face-centered cubes (FCC): atomic and electronic requirements of $[M_m(SR)_l(PR'_3)_8]^q$ nanoclusters (M = Coinage Metals) and their implications with respect to nucleation and growth of FCC metals, *Inorg. Chem.*, 2017, **56**, 11470.

71 H. Yang, J. Yan, Y. Wang, H. Su, L. Gell, X. Zhao, C. Xu, B. K. Teo, H. Häkkinen and N. Zheng, Embryonic growth of face-center-cubic silver nanoclusters shaped in nearly perfect half-cubes and cubes, *J. Am. Chem. Soc.*, 2017, **139**, 31–34.

72 Z.-Y. Wang, M.-Q. Wang, Y.-L. Li, P. Luo, T.-T. Jia, R.-W. Huang, S.-Q. Zang and T. C. W. Mak, Atomically precise site-specific tailoring and directional assembly of superatomic silver nanoclusters, *J. Am. Chem. Soc.*, 2018, **140**, 1069–1076.

73 J. Chai, S. Yang, Y. Lv, T. Chen, S. Wang, H. Yu and M. Zhu, A unique pair: Ag_{40} and Ag_{46} nanoclusters with the same surface but different cores for structure-property correlation, *J. Am. Chem. Soc.*, 2018, **140**, 15582–15585.

74 M. Bodiuzzaman, A. Ghosh, K. S. Sugi, A. Nag, E. Khatun, B. Varghese, G. Paramasivam, S. Antharjanam, G. Natarajan

and T. Pradeep, Camouflaging structural diversity: Co-crystallization of two different nanoparticles having different cores but the same shell, *Angew. Chem., Int. Ed.*, 2019, **58**, 189–194.

75 M. Alhilaly, M. Bootharaju, C. Joshi, T. Besong, A. Emwas, R. Juarez-Mosqueda, S. Kaappa, S. Malola, K. Adil, A. Shkurenko, H. Häkkinen, M. Eddaoudi and O. Bakr, $[Ag_{67}(SPhMe_2)_{32}(PPh_3)_8]^{3+}$: Synthesis, total structure, and optical properties of a large box-shaped silver nanocluster, *J. Am. Chem. Soc.*, 2016, **138**, 14727.

76 X. Yuan, C. Sun, X. Li, S. Malola, B. K. Teo, H. Häkkinen, L. Zheng and N. Zheng, Combinatorial identification of hydrides in a ligated Ag_{40} nanocluster with noncompact metal core, *J. Am. Chem. Soc.*, 2019, **141**, 11905–11911.

77 C. Zeng, C. Liu, Y. Chen, N. L. Rosi and R. Jin, Gold-thiolate ring as a protecting motif in the $Au_{20}(SR)_{16}$ nanocluster and implications, *J. Am. Chem. Soc.*, 2014, **136**, 11922–11925.

78 C. Zeng, T. Li, A. Das, N. L. Rosi and R. Jin, Chiral structure of thiolate-protected 28-gold-atom nanocluster determined by X-ray crystallography, *J. Am. Chem. Soc.*, 2013, **135**, 10011–10013.

79 C. Zeng, Y. Chen, K. Kirschbaum, K. Appavoo, M. Y. Sfeir and R. Jin, Structural patterns at all scales in a nonmetallic chiral $Au_{133}(SR)_{52}$ nanoparticle, *Sci. Adv.*, 2015, **1**, e1500045.

80 H. Yang, Y. Wang and N. Zheng, Stabilizing subnanometer Ag(0) nanoclusters by thiolate and diphosphine ligands and their crystal structures, *Nanoscale*, 2013, **5**, 2674–2677.

81 X. Zou, S. Jin, W. Du, Y. Li, P. Li, S. Wang and M. Zhu, Multi-ligand-directed synthesis of chiral silver nanoclusters, *Nanoscale*, 2017, **9**, 16800–16805.

82 H. Yang, J. Yan, Y. Wang, G. Deng, H. Su, X. Zhao, C. Xu, B. K. Teo and N. Zheng, From racemic metal nanoparticles to optically pure enantiomers in one pot, *J. Am. Chem. Soc.*, 2017, **139**, 16113–16116.

83 F. Tian and R. Chen, Pd-mediated synthesis of Ag_{33} chiral nanocluster with core-shell structure in T point group, *J. Am. Chem. Soc.*, 2019, **141**, 7107–7114.

84 H. Y. Yang, Y. Wang, X. Chen, X. J. Zhao, L. Gu, H. Q. Huang, J. Z. Yan, C. F. Xu, G. Li, J. C. Wu, A. J. Edwards, B. Dittrich, Z. C. Tang, D. D. Wang, L. Lehtovaara, H. Häkkinen and N. Zheng, Plasmonic twinned silver nanoparticles with molecular precision, *Nat. Commun.*, 2016, **7**, 12809–12816.

85 L. Ren, P. Yuan, H. Su, S. Malola, S. Lin, Z. Tang, B. K. Teo, H. Häkkinen, L. Zheng and N. Zheng, Bulky surface ligands promote surface reactivities of $[Ag_{141}X_{12}(S\text{-}Adm)_{40}]^{3+}$ (X = Cl, Br, I) nanoclusters: models for multiple-twinned nanoparticles, *J. Am. Chem. Soc.*, 2017, **139**, 13288–13291.

86 Y. B. Song, K. Lambright, M. Zhou, K. Kirschbaum, J. Xiang, A. D. Xia, M.-Z. Zhu and R. C. Jin, Large-scale synthesis, crystal structure, and optical properties of the $Ag_{146}Br_2(SR)_{80}$ nanocluster, *ACS Nano*, 2018, **12**, 9318–9325.

87 J. Z. Yan, J. Zhang, X. M. Chen, S. Malola, B. Zhou, E. Selenius, X. M. Zhang, P. Yuan, G. C. Deng, K. L. Liu, H. F. Su, B. K. Teo, H. Häkkinen, L. S. Zheng and N. Zheng, Thiol-stabilized atomically precise, superatomic silver nanoparticles for catalysing cycloisomerization of alkynyl amines, *Natl. Sci. Rev.*, 2018, **5**, 694–702.

88 J. Y. Liu, F. Alkan, Z. Wang, Z. Y. Zhang, M. Kurmoo, Z. Yan, Q. Q. Zhao, C. M. Aikens, C. H. Tung and D. Sun, Different silver nanoparticles in one crystal: $Ag_{210}(^{i}PrPhS)_{71}(Ph_3P)_5Cl$ and $Ag_{211}(^{i}PrPhS)_{71}(Ph_3P)_6Cl$, *Angew. Chem., Int. Ed.*, 2019, **58**, 195–199.

89 E. Khatun, M. Bodiuzzaman, K. S. Sugi, P. Chakraborty, G. Paramasivam, W. A. Dar, T. Ahuja, S. Antharjanam and T. Pradeep, Confining an Ag_{10} core in an Ag_{12} shell: a four-electron superatom with enhanced photoluminescence upon crystallization, *ACS Nano*, 2019, **13**, 5753–5759.

90 Z. Lei, X. K. Wan, S. F. Yuan, Z. J. Guan and Q. M. Wang, Alkynyl approach toward the protection of metal nanoclusters, *Acc. Chem. Res.*, 2018, **51**, 2465–2474.

91 Q.-M. Wang, Y.-M. Lin and K.-G. Liu, Role of anions associated with the formation and properties of silver clusters, *Acc. Chem. Res.*, 2015, **48**, 1570–1579.

92 Z. Lei, X.-K. Wan, S.-F. Yuan, J.-Q. Wang and Q.-M. Wang, Alkynyl-protected gold and gold-silver nanoclusters, *Dalton Trans.*, 2017, **46**, 3427–3434.

93 S.-F. Yuan, P. Li, Q. Tang, X.-K. Wan, Z.-A. Nan, D.-E. Jiang and Q.-M. Wang, Alkynyl-protected silver nanoclusters featuring an anticuboctahedral kernel, *Nanoscale*, 2017, **9**, 11405–11409.

94 Z.-J. Guan, F. Hu, S.-F. Yuan, Z.-A. Nan, Y.-M. Lin and Q.-M. Wang, The stability enhancement factor beyond eight-electron shell closure in thiacalix[4] arene-protected silver clusters, *Chem. Sci.*, 2019, **10**, 3360–3365.

95 Z.-J. Guan, J.-L. Zeng, Z.-A. Nan, X.-K. Wan, Y.-M. Lin and Q.-M. Wang, Thiacalix[4] arene: new protection for metal nanoclusters, *Sci. Adv.*, 2016, **2**, e1600323.

96 F. Hu, J.-J. Li, Z.-J. Guan, S.-F. Yuan and Q.-M. Wang, Formation of an alkynyl-protected silver nanocluster Ag_{112} promoted by in situ released chlorides from CH_2Cl_2, *Angew. Chem., Int. Ed.*, 2020, **59**, 5312–5315.

97 S.-S. Zhang, F. Alkan, H.-F. Su, C. M. Aikens, C.-H. Tung and D. Sun, $[Ag_{48}(C{\equiv}C^{t}Bu)_{20}(CrO_4)_7]$: An atomically precise silver nanocluster co-protected by inorganic and organic ligands, *J. Am. Chem. Soc.*, 2019, **141**, 4460–4467.

98 R. S. Dhayal, J.-H. Liao, Y.-C. Liu, M.-H. Chiang, S. Kahlal, J.-Y. Saillard and C. W. Liu, $[Ag_{21}\{S_2P(O^{i}Pr)_2\}^{12}]^{+}$: an eight-electron superatom, *Angew. Chem., Int. Ed.*, 2015, **54**, 3702.

99 R. S. Dhayal, Y.-R. Lin, J.-H. Liao, Y.-J. Chen, Y.-C. Liu, M.-H. Chiang, S. Kahlal, J.-Y. Saillard and C. W. Liu, $[Ag_{20}\{S_2P(OR)_2\}_{12}]$: a superatom complex with a chiral metallic core and high potential for isomerism, *Chem. – Eur. J.*, 2016, **22**, 9943.

100 W.-T. Chang, P.-Y. Lee, J.-H. Liao, K. K. Chakrahari, S. Kahlal, Y.-C. Liu, M.-H. Chiang, J.-Y. Saillard and C. W. Liu, Eight-electron silver and mixed gold/silver nanoclusters stabilized by selenium donor ligands, *Angew. Chem., Int. Ed.*, 2017, **56**, 10178–10182.

101 S.-F. Yuan, Z.-J. Guan, W.-D. Liu and Q.-M. Wang, Solvent-triggered reversible interconversion of all-nitrogen-donor-protected silver nanoclusters and their responsive optical properties, *Nat. Commun.*, 2019, **10**, 4032.

102 X.-T. Shen, X.-Li. Ma, Q.-L. Ni, M.-X. Ma, L.-C. Gui, C. Hou, R.-B. Hou and X.-J. Wang, $[Ag_{15}(N\text{-triphos})_4(Cl_4)](NO_3)_3$: a stable Ag-P superatom with eight electrons (N-triphos = tris ((diphenylphosphino) methyl) amine), *Nanoscale*, 2018, **10**, 515–519.

103 G.-X. Duan, J. Han, B.-Z. Yang, Y.-P. Xie and X. Lu, Oxometalate and phosphine ligand co-protected silver nanoclusters: $Ag_{28}(dppb)_6(MO_4)_4$ and $Ag_{32}(dppb)_{12}(MO_4)_4(NO_3)_4$, *Nanoscale*, 2020, **12**, 1617–1622.

104 J. Yan, H. Su, H. Yang, C. Hu, S. Malola, S. Lin, B.-K. Teo, H. Häkkinen and N. Zheng, Asymmetric synthesis of chiral bimetallic $[Ag_{28}Cu_{12}(SR)_{24}]^{4-}$ nanoclusters via ion pairing, *J. Am. Chem. Soc.*, 2016, **138**, 12751.

105 M. S. Bootharaju, H. Chang, G. Deng, S. Malola, W. Baek, H. Häkkinen, N. Zheng and T. Hyeon, $Cd_{12}Ag_{32}(SePh)_{36}$: non-noble metal doped silver nanoclusters, *J. Am. Chem. Soc.*, 2019, **141**, 8422.

106 K. Yonesato, H. Ito, H. Itakura, D. Yokogawa, T. Kikuchi, N. Mizuno, K. Yamaguchi and K. Suzuki, Controlled assembly synthesis of atomically precise ultrastable silver nanoclusters with polyoxometalates, *J. Am. Chem. Soc.*, 2019, **141**, 19550–19554.

107 Y.-M. Su, Z. Wang, G.-L. Zhuang, Q.-Q. Zhao, X.-P. Wang, C.-H. Tung and D. Sun, Unusual fcc-structured Ag_{10} kernels trapped in Ag_{70} nanoclusters, *Chem. Sci.*, 2019, **10**, 564–568.

108 J.-W. Liu, Z. Wang, Y.-M. Chai, M. Kurmoo, Q.-Q. Zhao, X.-P. Wang, C.-H. Tung and D. Sun, Core modulation of 70-nuclei core-shell silver nanoclusters, *Angew. Chem., Int. Ed.*, 2019, **58**, 6276–6279.

109 Z. Wang, H.-T. Sun, M. Kurmoo, Q.-Y. Liu, G.-L. Zhuang, Q.-Q. Zhao, X.-P. Wang, C.-H. Tung and D. Sun, Carboxylic acid stimulated silver shell isomerism in a triple core–shell Ag_{84} nanocluster, *Chem. Sci.*, 2019, **10**, 4862–4867.

110 T. Vosch, Y. Antoku, J.-C. Hsiang, C. I. Richards, J. I. Gonzalez and R. M. Dickson, Strongly emissive individual DNA-encapsulated Ag nanoclusters as single-molecule fluorophores, *Proc. Natl. Acad. Sci. U. S. A.*, 2007, **104**, 12616–12621.

111 D. Schultz, K. Gardner, S. S. R. Oemrawsingh, N. Markesevic, K. Olsson, M. Debord, D. Bouwmeester and E. Gwinn, Evidence for rod-shaped DNA-stabilized silver nanocluster emitters, *Adv. Mater.*, 2013, **25**, 2797–2803.

112 Z. Yuan, Y.-C. Chen, H.-W. Li and H.-T. Chang, Fluorescent silver nanoclusters stabilized by DNA scaffolds, *Chem. Commun.*, 2014, **50**, 9800–9815.

113 J. T. Petty, O. O. Sergev, M. Ganguly, I. J. Rankine, D. M. Chevrier and P. Zhang, A segregated, partially oxidized, and compact Ag_{10} cluster within an encapsulating DNA host, *J. Am. Chem. Soc.*, 2016, **138**, 3469–3477.

114 E. Thyrhaug, S. A. Bogh, M. R. Carro-Temboury, C. S. Madsen, T. Vosch and D. Zigmantas, Ultrafast coherence transfer in DNA-templated silver nanoclusters, *Nat. Commun.*, 2017, **8**, 15577.

115 J. M. Obliosca, C. Liu and H.-C. Yeh, Fluorescent silver nanoclusters as DNA probes, *Nanoscale*, 2013, **5**, 8443–8461.

116 W. Guo, J. Yuan, Q. Dong and E. Wang, Highly sequence-dependent formation of fluorescent silver nanoclusters in hybridized DNA duplexes for single nucleotide mutation identification, *J. Am. Chem. Soc.*, 2010, **132**, 932–934.

117 H.-C. Yeh, J. Sharma, J. J. Han, J. S. Martinez and J. H. Werner, A DNA–silver nanocluster probe that fluoresces upon hybridization, *Nano Lett.*, 2010, **10**, 3106–3110.

118 X. Liu, F. Wang, R. Aizen, O. Yehezkeli and I. Willner, Graphene oxide/nucleic-acid-stabilized silver nanoclusters: functional hybrid materials for optical aptamer sensing and multiplexed analysis of pathogenic DNAs, *J. Am. Chem. Soc.*, 2013, **135**, 11832–11839.

119 J. T. Petty, J. Zheng, N. V. Hud and R. M. Dickson, DNA-templated Ag nanocluster formation, *J. Am. Chem. Soc.*, 2004, **126**, 5207–5212.

120 E. G. Gwinn, P. O'Neill, A. J. Guerrero, D. Bouwmeester and D. K. Fygenson, Sequence-dependent fluorescence of DNA hosted silver nanoclusters, *Adv. Mater.*, 2008, **20**, 279–283.

121 P. R. O'Neill, K. Young, D. Schiffels and D. K. Fygenson, Few-atom fluorescent silver clusters assemble at programmed sites on DNA nanotubes, *Nano Lett.*, 2012, **12**, 5464–5469.

122 J. Li, X. Jia, D. Li, J. Ren, Y. Han, Y. Xia and E. Wang, Stem-directed growth of highly fluorescent silver nanoclusters for versatile logic devices, *Nanoscale*, 2013, **5**, 6131–6138.

123 W. Li, L. Liu, Y. Fu, Y. Sun, J. Zhang and R. Zhang, Effects of polymorphic DNA on the fluorescent properties of silver nanoclusters, *Photochem. Photobiol. Sci.*, 2013, **12**, 1864–1872.

124 J. Ai, W. Guo, B. Li, T. Li, D. Li and E. Wang, DNA G-quadruplex-templated formation of the fluorescent silver nanocluster and its application to bioimaging, *Talanta*, 2012, **88**, 450–455.

125 H. X. Xu and K. S. Suslick, Water-soluble fluorescent silver nanoclusters, *Adv. Mater.*, 2010, **22**, 1078–1082.

126 I. Diez and R. H. Ras, Fluorescent silver nanoclusters, *Nanoscale*, 2011, **3**, 1963–1970.

127 L. Shang, S. Dong and G. U. Nienhaus, Ultra-small fluorescent metal nanoclusters: synthesis and biological applications, *Nano Today*, 2011, **6**, 401–418.

128 S. J. Guo and E. K. Wang, Noble metal nanomaterials: controllable synthesis and application in fuel cells and analytical sensors, *Nano Today*, 2011, **6**, 240–264.

129 S. Choi, R. M. Dickson and J. Yu, Developing luminescent silver nanodots for biological applications, *Chem. Soc. Rev.*, 2012, **41**, 1867–1891.

130 B. Han and E. Wang, DNA-templated fluorescent silver nanoclusters, *Anal. Bioanal. Chem.*, 2012, **402**, 129–138.

131 J. T. Petty, S. P. Story, J.-C. Hsiang and R. M. Dickson, DNA-templated molecular silver fluorophores, *J. Phys. Chem. Lett.*, 2013, **4**, 1148–1155.

132 Y. Tao, M. Li, J. Ren and X. Qu, Metal nanoclusters: novel probes for diagnostic and therapeutic applications, *Chem. Soc. Rev.*, 2015, **44**, 8636–8663.

133 A. Latorre and A. Somoza, DNA-mediated silver nanoclusters: synthesis, properties and applications, *ChemBioChem*, 2012, **13**, 951–958.

134 Y. Chen, M. L. Phipps, J. H. Werner, S. Chakraborty and J. S. Martinez, DNA-templated metal nanoclusters: from

emergent properties to unique applications, *Acc. Chem. Res.*, 2018, **51**, 2756–2763.

135 R. Jiang, B. Li, C. Fang and J. Wang, Unraveling the evolution and nature of the plasmons in (Au core)-(Ag shell) nanorods, *Adv. Mater.*, 2014, **26**, 5274–5309.

136 L. M. Liz-Marźan, C. J. Murphy and J. Wang, Nanoplasmonics, *Chem. Soc. Rev.*, 2014, **43**, 3820–3822.

137 Q. B. Zhang, Y. N. Tan, J. P. Xie and J. Y. Lee, Colloidal synthesis of plasmonic metallic nanoparticles, *Plasmonics*, 2009, **4**, 9–22.

138 J. Huang, Y. Zhu, M. Lin, Q. Wang, L. Zhao, Y. Yang, K. X. Yao and Y. Han, Site-specific growth of Au-Pd alloy horns on Au nanorods: a platform for highly sensitive monitoring of catalytic reactions by surface enhancement Raman spectroscopy, *J. Am. Chem. Soc.*, 2013, **135**, 8552–8561.

139 T. H. Lee and R. M. Dickson, Discrete two-terminal single nanocluster quantum optoelectronic logic operations at room temperature, *Proc. Natl. Acad. Sci. U. S. A.*, 2003, **100**, 3043–3046.

140 I. Chakraborty, J. Erusappan, A. Govindarajan, K. S. Sugi, T. Udayabhaskararao, A. Ghosh and T. Pradeep, Emergence of metallicity in silver clusters in the 150 atom regime: a study of differently sized silver clusters, *Nanoscale*, 2014, **6**, 8024–8031.

141 L. A. Peyser, A. E. Vinson, A. P. Bartko and R. M. Dickson, Photoactivated fluorescence from individual silver nanoclusters, *Science*, 2001, **291**, 103–106.

142 S. Li, X.-S. Du, B. Li, J.-Y. Wang, G.-P. Li, G.-G. Gao and S.-Q. Zang, Atom-precise modification of silver(I) thiolate cluster by shell ligand substitution: a new approach to generation of cluster functionality and chirality, *J. Am. Chem. Soc.*, 2018, **140**, 594–597.

143 E. Khatun, A. Ghosh, P. Chakraborty, P. Singh, M. Bodiuzzaman, P. Ganesan, G. Nataranjan, J. Ghosh, S. K. Pal and T. Pradeep, A thirty-fold photoluminescence enhancement induced by secondary ligands in monolayer protected silver clusters, *Nanoscale*, 2018, **10**, 20033–20042.

144 M. S. Bootharaju, C. P. Joshi, M. R. Parida, O. F. Mohammed and O. M. Bakr, Templated atom-precise calvanic synthesis and structure elucidation of a $[Ag_{24}Au(SR)_{18}]^-$ nanocluster, *Angew. Chem., Int. Ed.*, 2016, **55**, 922–926.

145 J. Yan, H. Su, H. Yang, S. Malola, S. Lin, H. Häkkinen and N. Zheng, Total structure and electronic structure analysis of doped thiolated silver $[MAg_{24}(SR)_{18}]^{2-}$ (M = Pd, Pt) clusters, *J. Am. Chem. Soc.*, 2015, **137**, 11880–11883.

146 X. Kang, S. Chen, S. Jin, Y. Song, Y. Xu, H. Yu, H. Sheng and M. Zhu, Heteroatom effects on the optical and electrochemical properties of $Ag_{25}(SR)_{18}$ and its dopants, *ChemElectroChem*, 2016, **3**, 1261–1265.

147 Y. Liu, X. Chai, X. Cai, M. Chen, R. Jin, W. Ding and Y. Zhu, Central doping of a foreign atom into the silver cluster for catalytic conversion of CO_2 toward C−C bond formation, *Angew. Chem., Int. Ed.*, 2018, **57**, 9775–9779.

148 X. Liu, J. Yuan, C. Yao, J. Chen, L. Li, X. Bao, J. Yang and Z. Wu, Crystal and solution photoluminescence of $MAg_{24}(SR)_{18}$ (M = Ag/Pd/Pt/Au) nanoclusters and some implications for the photoluminescence mechanisms, *J. Phys. Chem. C*, 2017, **121**, 13848–13853.

149 M. S. Bootharaju, S. M. Kozlov, Z. Cao, A. Shkurenko, A. M. El-Zohry, O. F. Mohammed, M. Eddaoudi, O. M. Bakr, L. Cavallo and J.-M. Basset, Tailoring the crystal structure of nanoclusters unveiled high photoluminescence via ion pairing, *Chem. Mater.*, 2018, **30**, 2719–2725.

150 G. Soldan, M. A. Aljuhani, M. S. Bootharaju, L. G. AbdulHalim, M. R. Parida, A.-H. Emwas, O. F. Mohammed and O. M. Bakr, Gold doping of silver nanoclusters: a 26-Fold enhancement in the luminescence quantum yield, *Angew. Chem., Int. Ed.*, 2016, **55**, 5749–5753.

151 S.-S. Zhang, L. Feng, R. D. Senanayake, C. M. Aikens, X.-P. Wang, Q.-Q. Zhao, C.-H. Tung and D. Sun, Diphosphine-protected ultrasmall gold nanoclusters: opened icosahedral Au_{13} and heart-shaped Au_8 clusters, *Chem. Sci.*, 2018, **9**, 1251–1258.

152 Y.-M. Su, H.-F. Su, Z. Wang, Y.-A. Li, S. Schein, Q.-Q. Zhao, X.-P. Wang, C.-H. Tung, D. Sun and L.-S. Zheng, Three silver nests capped by thiolate/phenylphosphonate, *Chem. – Eur. J.*, 2018, **24**, 15096–15103.

153 J.-W. Liu, L. Feng, H.-F. Su, Z. Wang, Q.-Q. Zhao, X.-P. Wang, C.-H. Tung, D. Sun and L.-S. Zheng, Anisotropic assembly of Ag_{52} and Ag_{76} nanoclusters, *J. Am. Chem. Soc.*, 2018, **140**, 1600–1603.

154 J.-W. Liu, H.-F. Su, Z. Wang, Y.-A. Li, Q.-Q. Zhao, X.-P. Wang, C.-H. Tung, D. Sun and L.-S. Zheng, A giant 90-nucleus silver cluster templated by hetero-anions, *Chem. Commun.*, 2018, **54**, 4461–4464.

155 X.-Y. Li, Z. Wang, H.-F. Su, S. Feng, M. Kurmoo, C.-H. Tung, D. Sun and L.-S. Zheng, Anion-templated nanosized silver clusters protected by mixed thiolate and diphosphine, *Nanoscale*, 2017, **9**, 3601–3608.

156 Z. Wang, H.-F. Su, Y.-Z. Tan, S. Schein, S.-C. Lin, W. Liu, S.-A. Wang, W.-G. Wang, C.-H. Tung, D. Sun and L.-S. Zheng, Assembly of silver trigons into a buckyball-like Ag_{180} nanocage, *Proc. Natl. Acad. Sci. U. S. A.*, 2017, **114**, E10505.

157 S.-S. Zhang, H.-F. Su, G.-L. Zhuang, X.-P. Wang, C.-H. Tung, D. Sun and L.-S. Zheng, A hexadecanuclear silver alkynyl cluster based NbO framework with triple emissions from the visible to near-infrared II region, *Chem. Commun.*, 2018, **54**, 11905–11908.

158 Z. Wang, H.-F. Su, M. Kurmoo, C.-H. Tung, D. Sun and L.-S. Zheng, Trapping an octahedral Ag_6 kernel in a seven-fold symmetric Ag_{56} nanowheel, *Nat. Commun.*, 2018, **9**, 2094.

159 Z. Wang, H.-F. Su, C.-H. Tung, D. Sun and L.-S. Zheng, Deciphering synergetic core-shell transformation from $[Mo_6O_{22}@Ag_{44}]$ to $[Mo_8O_{28}@Ag_{50}]$, *Nat. Commun.*, 2018, **9**, 4407.

160 R.-W. Huang, Y.-S. Wei, X.-Y. Dong, X.-H. Wu, C.-X. Du, S.-Q. Zang and T. C. W. Mak, Hypersensitive dual-function luminescence switching of a silver-chalcogenolate cluster-based metal-organic framework, *Nat. Chem.*, 2017, **9**, 689–697.

161 R.-W. Huang, X.-Y. Dong, B.-J. Yan, X.-S. Du, D.-H. Wei, S.-Q. Zang and T. C. W. Mak, Tandem silver cluster

isomerism and mixed linkers to modulate the photoluminescence of cluster-assembled materials, *Angew. Chem., Int. Ed.*, 2018, **57**, 8560–8566.

162 X.-Y. Dong, H.-L. Huang, J.-Y. Wang, H.-Y. Li and S.-Q. Zang, A flexible fluorescent SCC-MOF for switchable molecule identification and temperature display, *Chem. Mater.*, 2018, **30**, 2160–2167.

163 Q.-Q. Xu, X.-Y. Dong, R.-W. Huang, B. Li, S.-Q. Zang and T. C. W. Mak, A thermochromic silver nanocluster exhibiting dual emission character, *Nanoscale*, 2015, **7**, 1650–1654.

164 B. Li, R.-W. Huang, J.-H. Qin, S.-Q. Zang, G.-G. Gao, H.-W. Hou and T. C. W. Mak, Thermochromic luminescent nest-like silver thiolate cluster, *Chem. – Eur. J.*, 2014, **20**, 12416–12420.

165 X.-J. Xi, J.-S. Yang, J.-Y. Wang, X.-Y. Dong and S.-Q. Zang, New stable isomorphous Ag_{34} and Ag_{33} Au nanoclusters with an open shell electronic structure, *Nanoscale*, 2018, **10**, 21013–21018.

